

Supplementary Information

B–B Multiple Bonds-Mediated Dinitrogen Cleavage Induced by Carbon Monoxide

Chunwen Pan,^a Jin Hu,^a Liyan Cai,^a and Xuefeng Wang*^a

^a School of Chemical Science and Engineering, Shanghai Key Lab of Chemical Assessment and Sustainability, Tongji University, Shanghai, 200092, China.

E-mail: xfwang@tongji.edu.cn

Table of Contents

Experimental and theoretical methods	3
Supplementary Notes	4
Assignment of species <i>D</i> (BNCO) and <i>E</i> (NBCO)	4
Reaction potential energy surface of species <i>D</i> (BNCO) and <i>E</i> (NBCO)	4
Bonding analyses of species <i>A-E</i>	4
References	6
Supplementary Figures	7
Fig. S1. Infrared spectra of laser-ablated ¹⁰ B-enriched boron atoms with 1% CO in the N ₂ matrix.	7
Fig. S2. Infrared spectra of laser-ablated ¹⁰ B-enriched or nature boron atoms with 1% CO in the N ₂ matrix.	8
Fig. S3. Infrared spectra of laser-ablated ¹⁰ B-enriched boron atoms with 1% CO in the ¹⁵ N ₂ matrix.	9
Fig. S4. Infrared spectra of laser-ablated ¹⁰ B-enriched boron atoms with 1% ¹³ CO in the N ₂ matrix.	10
Fig. S5. Infrared spectra of laser-ablated ¹⁰ B-enriched boron atoms with 1% C ¹⁸ O in the N ₂ matrix.	11
Fig. S6. Infrared spectra of laser-ablated ¹⁰ B-enriched boron atoms with CO in isotopic nitrogen matrix.	12
Fig. S7. Infrared spectra of laser-ablated ¹⁰ B-enriched boron atoms with CO/ ¹³ CO in the N ₂ matrix.	13
Fig. S8. Infrared spectra of laser-ablated ¹⁰ B-enriched boron atoms with CO/C ¹⁸ O in the N ₂ matrix.	14
Fig. S9. Infrared spectra of laser-ablated natural boron atoms with 1% ¹³ CO in the N ₂ matrix.	15
Fig. S10. Infrared spectra of laser-ablated natural boron atoms with 1% C ¹⁸ O in the N ₂ matrix.	15
Fig. S11. Potential Energy Surface of BNBNCO from TS5.	16
Fig. S12. Transition state structures for the reaction from NNBBCO to (η^2 -N ₂)BBCO and BNBNCO and their frequencies.	16
Fig. S13. Qualitative bonding scheme of the frontier molecular orbitals of II.	17
Fig. S14. Charges on atoms of stationary points along the isomerization process of NNBBCO to BNBNCO.	17
Fig. S15. Potential energy surface for the reaction from NNBBNN to (η^2 -N ₂)BBNN and BNBNN + N ₂ .	18
Fig. S16. Charges on B–B center of stationary points along the isomerization process of NNBBNN or NNBBCO.	18
Fig. S17. Potential energy surface for the reaction of NNBN with CO to form NBCO (<i>E</i>) and BNCO (<i>D</i>).	18

Fig. S18. Selected frontier molecular orbitals of NNBBCO (<i>A</i>).	19
Fig. S19. Selected frontier molecular orbitals of (η^2 -N ₂)BBCO (<i>B</i>).	19
Fig. S20. Selected frontier molecular orbitals of BNBNCO (<i>A</i>).	20
Fig. S21. Plot of the deformation densities $\Delta\rho$ of BNBNCO ($^1\Sigma$) taking [BNB ⁺] ($^1\Sigma$) and [NCO ⁻] ($^1\Sigma$) as interacting fragments.	20
Fig. S22. Selected frontier molecular orbitals of BNCO (<i>D</i>).	21
Fig. S23. Selected frontier molecular orbitals of NBCO (<i>E</i>).	21
Supplementary Tables	22
Table S1. Observed and calculated infrared absorptions and intensities for isotopomers of products <i>A-E</i> in the reactions of ¹⁰ B with CO in the N ₂ matrix.	22
Table S2. Comparisons between experimental and calculated vibrational frequencies and isotopic frequency ratios of products <i>A-E</i> in the reactions of boron with CO in the N ₂ matrix.	23
Table S3. Observed and calculated infrared absorptions and intensities for isotopomers of products <i>A-E</i> in the reactions of ¹⁰ B with CO in the N ₂ matrix	24
Table S4. Observed and calculated infrared absorptions and intensities for isotopomers of products <i>A-E</i> in the reactions of ¹⁰ B with CO in the N ₂ matrix.	25
Table S5. Comparisons between experimental and calculated vibrational frequencies and isotopic frequency ratios of products <i>A-E</i> in the reactions of ¹¹ B with CO in the ¹⁴ N ₂ matrix.	26
Table S6. Orbital composition analysis on the I1 ($^1A'$) complex by Natural Atomic Orbital method.	27
Table S7. EDA-NOCV results of I1 ($^1A'$) taking BBCO ($^1A'$) and N ₂ ($^1\Sigma_g$) as interacting fragments.	28
Table S8. EDA-NOCV results of I1 ($^1A'$) taking BBCO and N ₂ in the different charged states as interacting fragments.	29
Table S9. The natural charge from Natural Population Analysis throughout the generation process of BNBNCO form NNBBCO.	30
Table S10. The natural charge from Natural Population Analysis throughout the generation process of BNB + N ₂ form NNBBNN.	31
Table S11. Calculated bond orders given by the Mayer method and Wiberg method.	32
Table S12. Orbital composition analysis on the BNBNCO complex by Natural Atomic Orbital method.	33
Table S13. EDA-NOCV results of BNBNCO ($^1\Sigma$) taking [BNB ⁺] ($^1\Sigma$) and [NCO ⁻] ($^1\Sigma$) as interacting fragments.	34
Table S14. Experimental frequencies of boron carbonyl compounds observed in the N ₂ matrix.	34
Table S15. Experimental frequencies of boron nitrides observed in the N ₂ matrix.	35
Table S16. Experimental frequencies of the products of boron atom react with CO and N ₂ in the N ₂ matrix.	36
Table S17. Observed and calculated (at the B3LYP/def2-TZVPP and CCSD(T)/cc-pVDZ levels) infrared absorptions for products <i>A-C</i> in the reactions of ¹¹ B with CO in the N ₂ matrix.	37

Methods

Experimental methods. Laser-ablated boron atoms and clusters, generated in an excess of nitrogen, were condensed at 4 K using a closed-cycle helium refrigerator (Sumitomo Heavy Industries Model SRDK-408D2). A neodymium-doped yttrium aluminum garnet (Nd:YAG) laser, operating at a fundamental wavelength of 1064 nm with a 10 Hz repetition rate and a pulse width of 10 ns, was directed onto a rotating boron target. The laser energy was meticulously adjusted within the range of 10-15 mJ/pulse. The ablated boron, enriched with ^{10}B (Eagle Pitcher, 93.8% ^{10}B and 6.2% ^{11}B) and natural boron (Eagle Pitcher, 80.4% ^{11}B and 19.6% ^{10}B), was allowed to react with carbon monoxide (CO) and its isotopomers, ^{13}CO (Cambridge Isotope Laboratories, Inc., 99 atom %), C^{18}O (Aldrich chemistry, 99 atom %), in an excess nitrogen matrix uniformly spread onto a CsI window. Isotopic $^{15}\text{N}_2$ (Cambridge Isotope Laboratories, 98%+) and $^{14}\text{N}_2 + ^{15}\text{N}_2$ mixtures were used in different experiments. Infrared spectra were captured at a resolution of 0.5 cm^{-1} across the range between 4000 and 400 cm^{-1} using a HgCdTe detector. The matrix samples underwent annealing at various temperatures, and select samples were exposed to photolysis using either a light-emitting diode (LED, 3 W) or a medium-pressure mercury arc lamp (Philips, 175 W) with the protective globe removed.

Theoretical Methods. All molecular structure optimizations and single-point energy calculations were executed at the B3LYP level, in conjunction with the def2-TZVPP basis set,^{1,2} utilizing the Gaussian 09 program.³ Transition states were refined using the Rational Function Optimization (RFO) method and authenticated through intrinsic reaction coordinate (IRC) calculations to ensure connectivity between the desired reactants and products. The Mayer bond order and Wiberg bond index were calculated to elucidate the bonding characteristics, employing the Multiwfn code^{4,5} in conjunction with the Gaussian 09 program. The orbital composition was determined through a natural bond orbital (NBO) population analysis.⁶ The orbital composition analysis was based on natural atomic orbital (NAO)⁷ and energy decomposition analysis combined with natural orbitals for chemical valence (EDA-NOCV).^{8,9} Visual representations of the frontier orbitals were crafted using the Multiwfn code and VMD program.¹⁰

Supplementary Notes

Assignment of Species **D** (BNCO) and **E** (NBCO)

The absorption bands of species **D** at 2294.5 cm⁻¹ and 1584.4 cm⁻¹ are attributed to the BNCO complex. The band at 2294.5 cm⁻¹ is indicative of the N–C–O stretching region, and its isotopic patterns derived from mixed isotopic-labeled samples (Figs. S6-S8) confirm the presence of a single NCO subunit. The band at 1584.4 cm⁻¹ demonstrates significant isotopic shifts of B-11 and N-15, yielding ¹⁰B/¹¹B and ¹⁴N/¹⁵N isotopic ratios of 1.0049 and 1.0218, respectively. The absence of band splitting in the natural boron experiment (Fig. S2b) suggests the involvement of a single boron atom. Collectively, the bands' positions and isotopic signatures indicate that this group of absorptions can be ascribed to BNCO (**D**), which is predicted to possess a ¹A' ground state with C_s symmetry at the B3LYP/def2-TZVPP level (Fig. S17). For species **E**, a new band at 2160.2 cm⁻¹ exhibits minimal isotopic shifts for N-15 and B-11 but significant shifts for C-13 and O-18 (Table S1), indicative of a terminal C–O stretching vibration. The band's 4/1 splits in the natural boron experiment at 2156.5 cm⁻¹ (¹¹B¹¹B) and 2160.2 cm⁻¹ (¹⁰B¹⁰B) (Fig. S2a and Table S3) support the involvement of a single boron atom. Consequently, species **E** is assigned to NBCO, which is predicted to have a ¹Σ ground state with linear structure at the B3LYP/def2-TZVPP level (Fig. S17). The calculated C–O stretching mode is 2174.4 cm⁻¹, which aligns well with the experimental value of 2160.2 cm⁻¹. The calculated B–N stretching mode of 1939.3 cm⁻¹ was not observed, possibly due to its weak intensity.

Reaction Potential Energy Surface

For the formation of the BNCO (**D**), we have explored the reaction of NNBN (from BN + N₂), which decreased under UV-vis (λ > 220 nm) coinciding with the increase of **D**, with CO molecule (Fig. S17). The reaction is exothermic by 41.6 kcal/mol at the B3LYP/def2-TZVPP level. Both BNCO (**D**) and NBCO (**E**) form during deposition and intensify at 25 K annealing. Under UV-vis (λ > 220 nm) irradiation, **E** was observed to decrease while **D** increased. This implies that complex **E** isomerizes to complex **D**, which is endothermic with a predicted energy decrease of 15.4 kcal/mol and proceeds via a transition state TS2, which is 29.2 kcal/mol higher in energy than complex **D**.

Bonding analyses of species **A-E**

Valuable insights into the bonding scenarios within the molecules are derived from the atomic charge distribution, as depicted in Fig. 2. The least electronegative boron atoms carry, as expected, large positive charges in complex **C** (0.44 e and 1.18 e). The positive charges on the boron atoms are significantly smaller in complex **B** (0.37 e and 0.10 e) and one of them carries even a negative charge in complex **A** (0.17 e and -0.26 e). Such an atypical charge distribution was previously reported for molecules where boron acts as a Lewis acid, binding to donor ligands such as CAAC¹¹ or CO¹². This distribution suggests that complexes **A** and **B** can be classified as donor-acceptor complexes of B₂ with the ligands CO and end-on or side-on bonded N₂. Molecular orbitals of NNBBBCO (**A**) (Fig. S18) provide further clarity on the bonding nature. The doubly degenerate HOMO and HOMO-1 represent B–B π bonding orbitals, indicative of B₂ π → CO/N₂ π* back-bonding. The HOMO-2 is a B–B σ bonding orbital, while HOMO-9 and HOMO-10 comprise CO σ → B₂ σ donation and NN σ → B₂ σ donation. This pattern suggests that singlet NNBBBCO (**A**) exhibits characteristics of a B≡B triple bond, with a Lewis structure of N≡N–B≡B–C≡O, and features B₂ to CO/N₂ back bonding via delocalization of the electron density of the two π bonds of B₂ into the π* orbital of the CO or N₂ ligand. The C–O bonds in NNBBBCO (**A**) and (η²-N₂)BBCO (**B**) are slightly elongated to 1.150 Å and 1.163 Å, respectively, compared to that in a free CO molecule (1.125 Å). In (η²-N₂)BBCO (**B**), the N–N and B–B distances are substantially longer (N–N:1.263 Å, B–B:1.582 Å, respectively) compared to NNBBBCO (**A**) (N–N:1.127 Å, B–B:1.442 Å). This difference corresponds to reduced Mayer bond orders for (η²-N₂)BBCO (**B**) (N–N:1.58, B–B:1.13) versus NNBBBCO (**A**) (N–N:2.10, B–B:1.94), as detailed in Table S11. The ground state of (η²-N₂)BBCO was found to be a ³A₂ ground state with C_{2v} symmetry. The C_{2v} triplet is 1.3 kcal/mol lower than a C_{2v} singlet at the B3LYP/def2-TZVPP level (0.4 kcal/mol at CCSD (T)/def2-TZVPP level). The singly occupied molecular orbital

(SOMO) and SOMO-1 of triplet (η^2 -N₂)BBCO (**B**) are indicative of π^* bonding and π bonding of the B–B back-donation to the CO antibonding π^* orbital (Fig. S19), which are similar to the π back-donation of B₂ to CO π^* in the 2 π MO of linear triplet BBCO.¹³ Additionally, the HOMO-2 represents B–B π back-donation to the antibonding π^* orbital of side-on N₂, leading to elongated N–N and B–B bond lengths. The HOMO-3 and HOMO-4 denote the N–N σ bond and B–B σ bond, while HOMO-11 represents σ bonding orbital of B–CO, respectively, which involve π bonding orbital of side-on N₂ and the σ orbital of the CO donating to B–B σ orbitals.

The BNBNC O (**C**) molecule possesses $C_{\infty v}$ symmetry in the $^1\Sigma$ ground state with linear structure. The B₁–N₁ and B₂–N₂ bond lengths, as calculated at the B3LYP/def-TZVPP level, are 1.359 Å and 1.349 Å (Fig. 2), respectively, which are close to those of a B=N double bond (1.39 Å).^{14,15} The N₁–B₂ bond (1.271 Å) potentially exhibits triple bond character, akin to the B≡N triple bond length in iminoborane (1.26 Å).¹⁵ The calculated Mayer bond orders for B₁–N₁ and B₂–N₂ are 1.25 and 1.41, respectively, while the bond order for N₁–B₂ is higher at 2.10 (Table S11). The molecular orbitals of BNBNC O, depicted in Fig. S20, in conjunction with the NAO method (Table S12), reveal the bonding nature. The HOMO reflects lone pair electrons on boron (B₁), while the doubly degenerate HOMO-1 and HOMO-2 represent three-center-two-electrons π bonding across B₁–N₁–B₂, consisting of the 2 p orbitals of B₁ and B₂ and 2 p orbitals of N₁. This pattern continues with the doubly degenerate HOMO-3 and HOMO-4, which denote π bonding across N₁–B₂–N₂, consisting of the 2 p orbitals of B₂ and 2 p orbitals of N₁ and N₂. The N₁–B₂ bond, situated at the overlap of four π bonds, corresponds to a shorter N₁–B₂ bond length and a larger N₁–B₂ bond order, consistent with previous results. The doubly degenerate HOMO-5 and HOMO-6 represent π bonding across N–C–O with calculated Mayer bond orders of 1.99 for N–C and 2.16 for C–O. The extensive π bonding across the linear molecule endows BNBNC O with high stability, and theoretical calculations confirm that it serves as the most stable structure among all isomers, as shown in Fig. 3. The calculated charge distribution given in Fig. 2 suggests that the bonding situation in **C** is best discussed using NBN⁺ cation and NCO[−] anion as interacting fragments. The EDA-NOCV results for **C** using NBN⁺ and NCO[−] as fragments give a straightforward picture of the bonds (Table S13). Fig. S21 shows the associated charge flow of the σ and π donation and the orbitals of the fragments. The largest stabilization caused by orbital interactions is due to the σ donation of the HOMO-1 (7 σ MO) of the isocyanate anion into the LUMO (7 σ MO) of NBN⁺ cation followed by the π donation of the degenerate HOMO (2 π MOs) of the isocyanate anion into the degenerate LUMO+1 (2 π MOs) of NBN⁺ cation.

The B–N bond lengths in BNCO (**D**) and NBCO (**E**) are 1.376 Å and 1.260 Å calculated at the B3LYP/def-TZVPP level, respectively, which are close to those of B=N double bond (1.39 Å) and B≡N triple bond length in iminoborane (1.26 Å).^{14,15} As depicted in the molecular orbitals shown in Fig. S22, the BNCO (**D**) molecule possesses a lone pair of electrons on B (HOMO) similar to BNBNC O (**C**), as well as two equivalent π bonds across N–C–O (HOMO-3 and HOMO-4). The molecular orbital of NBCO (**E**) depicted in Fig. S23, which shows the degenerate HOMO, HOMO-1, and HOMO-2, clearly indicates the N≡B triple bond, comprising two π bonds and one σ bond.

References

- 1 A. D. Becke, *J. Chem. Phys.*, 1993, **98**, 5648–5652.
- 2 C. Lee, W. Yang and R. G. Parr, *Phys. Rev. B*, 1988, **37**, 785–789.
- 3 Gaussian 09 Citation | Gaussian.com, <https://gaussian.com/g09citation/>, (accessed April 9, 2024).
- 4 T. Lu and F. Chen, *J. Comput. Chem.*, 2012, **33**, 580–592.
- 5 T. Lu, *J. Chem. Phys.*, 2024, **161**, 082503.
- 6 A. E. Reed, R. B. Weinstock and F. Weinhold, *J. Chem. Phys.*, 1985, **83**, 735–746.
- 7 E. D. Glendening, C. R. Landis and F. Weinhold, *WIREs Comput. Mol. Sci.*, 2012, **2**, 1–42.
- 8 L. Zhao, S. Pan, N. Holzmann, P. Schwerdtfeger and G. Frenking, *Chem. Rev.*, 2019, **119**, 8781–8845.
- 9 J. Andrés, P. W. Ayers, R. A. Boto, R. Carbó-Dorca, H. Chermette, J. Cioslowski, J. Contreras-García, D. L. Cooper, G. Frenking, C. Gatti, F. Heidar-Zadeh, L. Joubert, Á. Martín Pendás, E. Matito, I. Mayer, A. J. Misquitta, Y. Mo, J. Pilmé, P. L. A. Popelier, M. Rahm, E. Ramos-Cordoba, P. Salvador, W. H. E. Schwarz, S. Shahbazian, B. Silvi, M. Solà, K. Szalewicz, V. Tognetti, F. Weinhold and É.-L. Zins, *J. Comput. Chem.*, 2019, **40**, 2248–2283.
- 10 W. Humphrey, A. Dalke and K. Schulten, *J. Mol. Graph.*, 1996, **14**, 33–38.
- 11 R. Kinjo, B. Donnadieu, M. A. Celik, G. Frenking and G. Bertrand, *Science*, 2011, **333**, 610–613.
- 12 H. Braunschweig, R. D. Dewhurst, F. Hupp, M. Nutz, K. Radacki, C. W. Tate, A. Vargas and Q. Ye, *Nature*, 2015, **522**, 327–330.
- 13 M. Zhou, Z.-X. Wang, P. von Ragué Schleyer and Q. Xu, *Chem. Phys. Chem.*, 2003, **4**, 763–766.
- 14 S. Berski, Z. Latajka and A. J. Gordon, *New J. Chem.*, 2011, **35**, 89–96.
- 15 P. Paetzold, *Adv. Inorg. Chem.*, 1987, **31**, 123–170.

Supplementary Figures

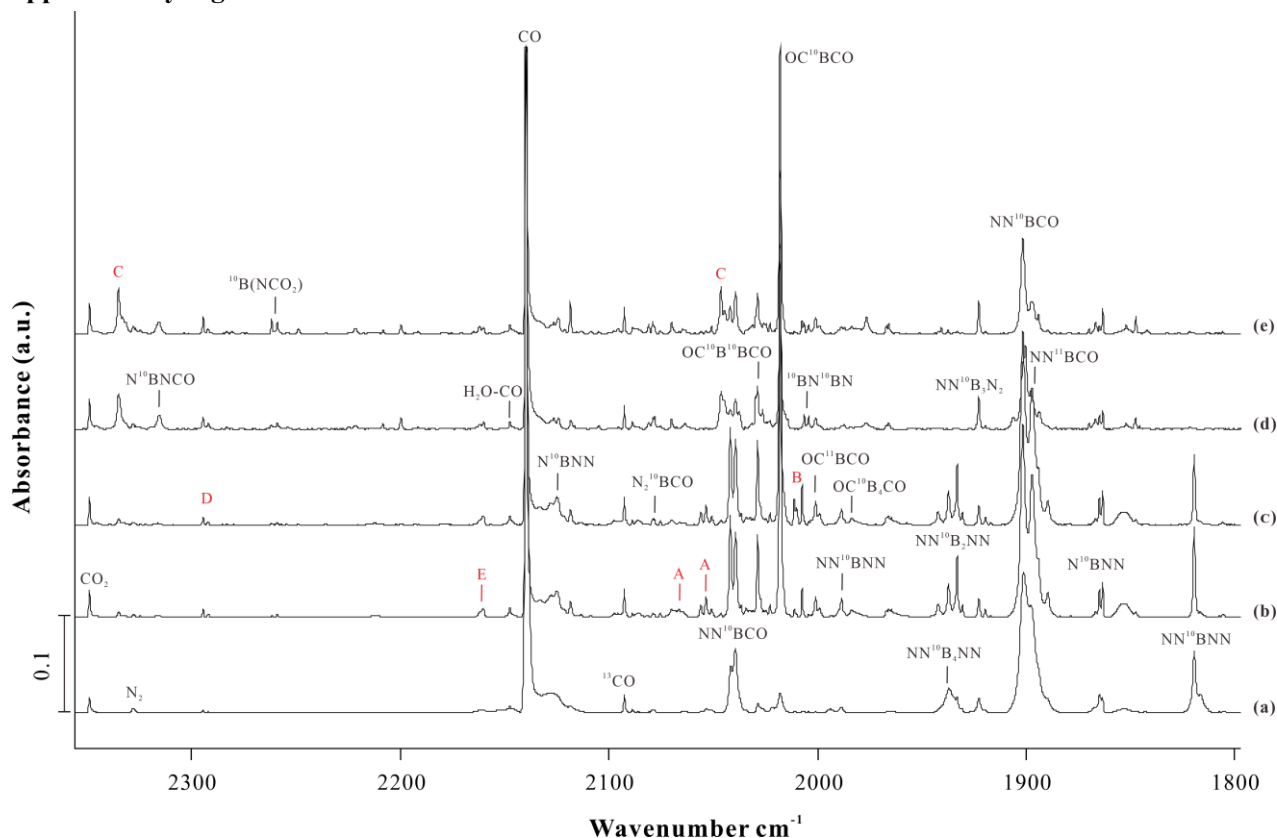


Fig. S1a. Infrared spectra in the 2350 cm⁻¹-1800 cm⁻¹ region of laser-ablated ¹⁰B-enriched boron atoms with 1% CO in the N₂ matrix. (a) co-deposition at 4 K for 1 h; (b) after annealing to 25 K; (c) after 450 nm irradiation for 10 min; (d) after >220 nm irradiation for 10 min; (e) after annealing to 30 K. [A: NNBBCO, B: (η^2 -N₂)BBCO, C: BNBBCO, D: BNCO, E: NBCO].

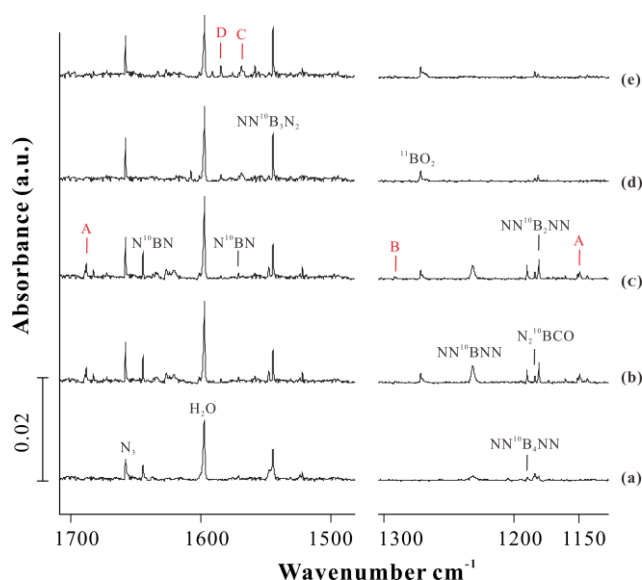


Fig. S1b. Infrared spectra in the 1700-1500 cm^{-1} , 1300-1150 cm^{-1} regions of laser-ablated ^{10}B -enriched boron atoms with 1% CO in the N_2 matrix. (a) co-deposition at 4 K for 1 h; (b) after annealing to 25 K; (c) after 450 nm irradiation for 10 min; (d) after >220 nm irradiation for 10 min; (e) after annealing to 30 K. [A: NNBCO, B: $(\eta^2\text{-N}_2)\text{BBCO}$, C: BNBNCO, D: BNCO].

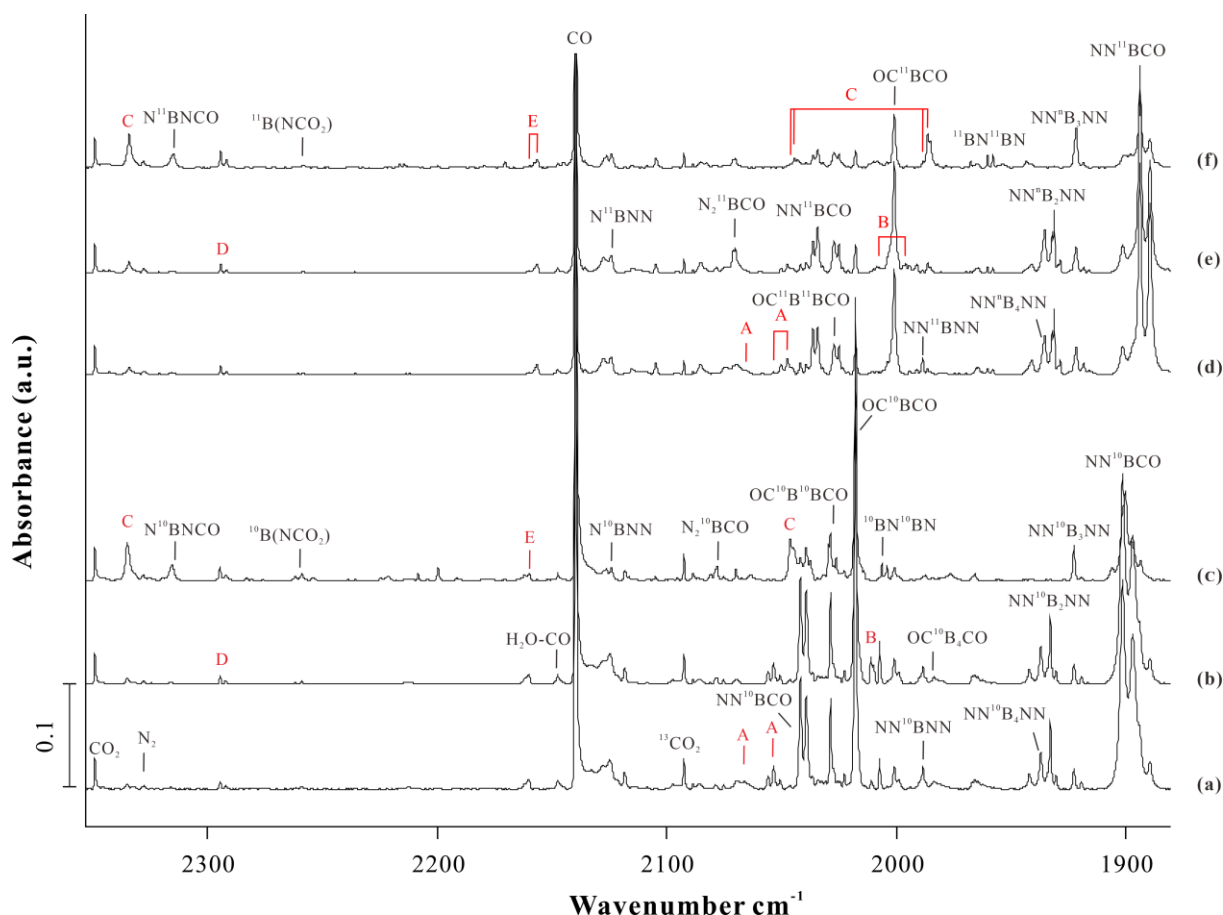


Fig. S2a. Infrared spectra in the 2350-1850 cm⁻¹ region of laser-ablated ¹⁰B-enriched or natural boron atoms with 1% CO in the N₂ matrix. ¹⁰B + 1% CO in N₂: (a) after annealing to 25 K; (b) after 450 nm irradiation for 10 min; (c) after >220 nm irradiation for 10 min; ¹¹B + 1% CO in N₂: (d) after annealing to 25 K; (e) after 450 nm irradiation for 10 min; (f) after >220 nm irradiation for 10 min. [A: NNBBBCO, B: (η²-N₂)BBCO, C: BNBBCO, D: BNCO, E: NBCO].

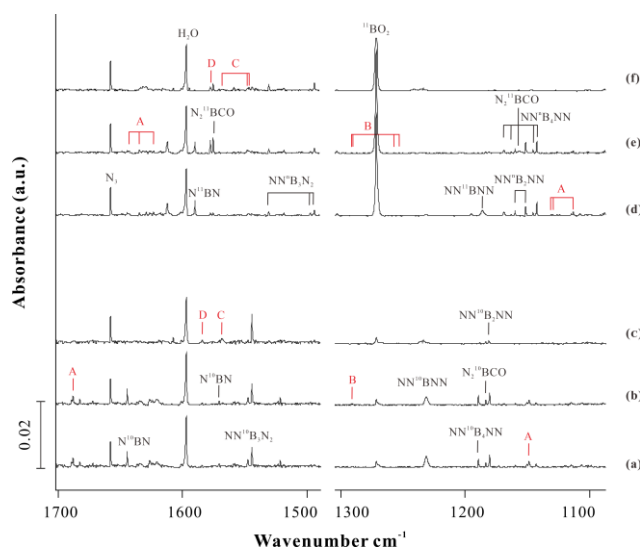
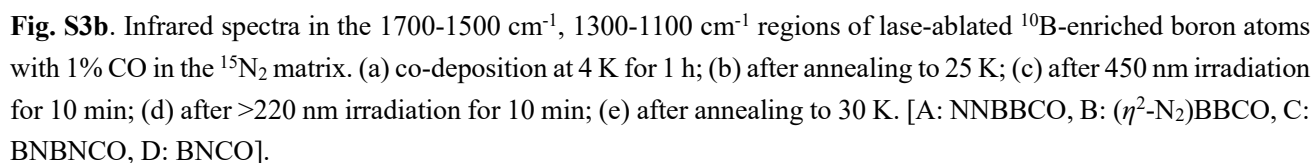
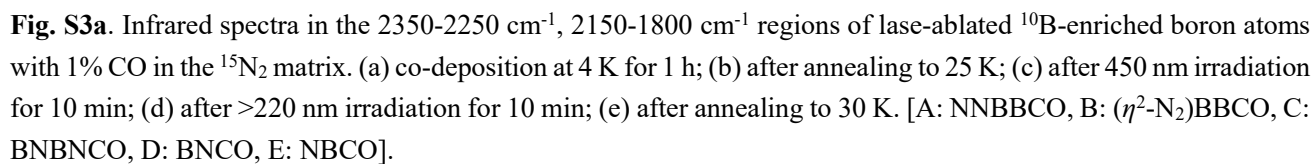


Fig. S2b. Infrared spectra in the 1700-1100 cm⁻¹ region of laser-ablated ¹⁰B-enriched or natural boron atoms with 1% CO in the N₂ matrix. ¹⁰B + 1% CO in N₂: (a) after annealing to 25 K; (b) after 450 nm irradiation for 10 min; (c) after >220 nm irradiation for 10 min; ¹¹B + 1% CO in N₂: (d) after annealing to 25 K; (e) after 450 nm irradiation for 10 min; (f) after >220 nm irradiation for 10 min. [A: NNBBBCO, B: (η²-N₂)BBCO, C: BNBBCO, D: BNCO].



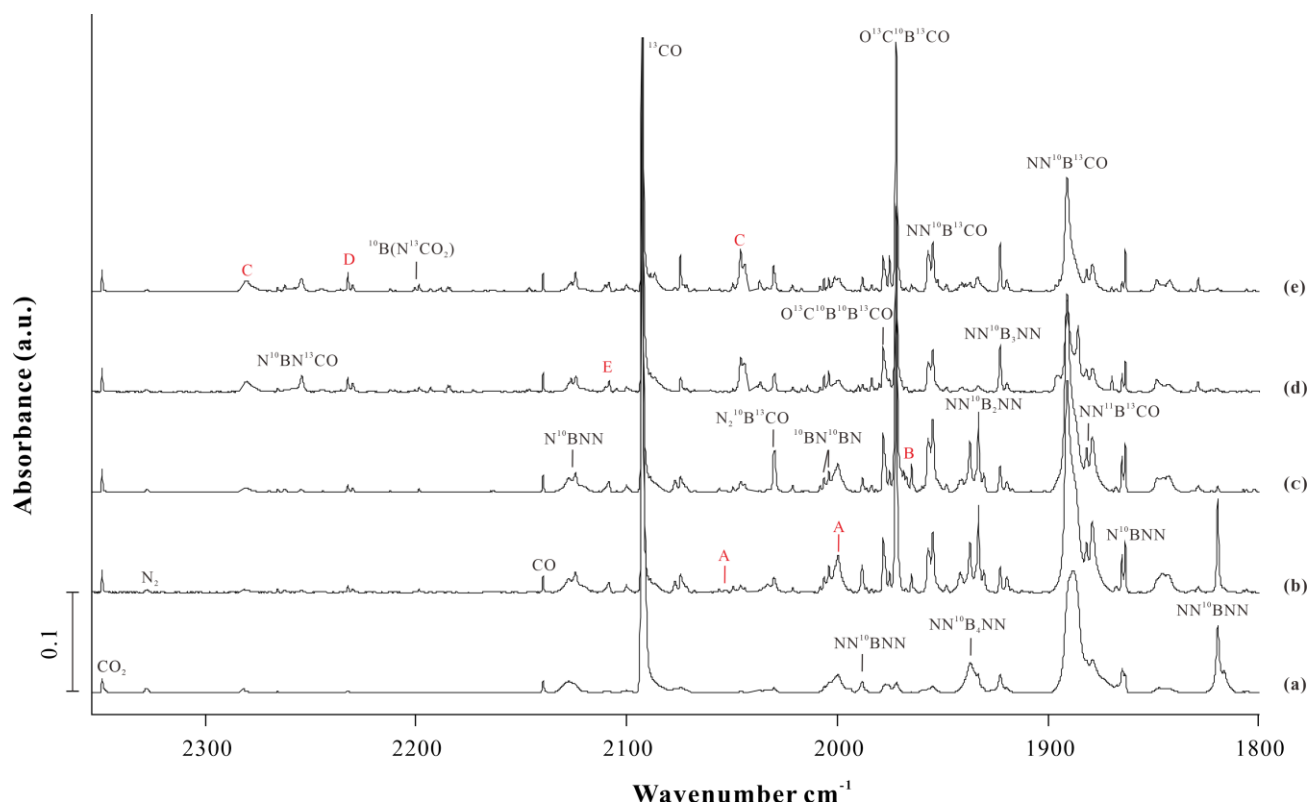


Fig. S4a. Infrared spectra in the 2350-1800 cm^{-1} region of laser-ablated ^{10}B -enriched boron atoms with 1% ^{13}CO in the N_2 matrix. (a) co-deposition at 4 K for 1 h; (b) after annealing to 25 K; (c) after 450 nm irradiation for 10 min; (d) after >220 nm irradiation for 10 min; (e) after annealing to 30 K. [A: NNBB CO , B: $(\eta^2\text{-N}_2)\text{BBCO}$, C: BNB NCO , D: BN CO , E: NB CO].

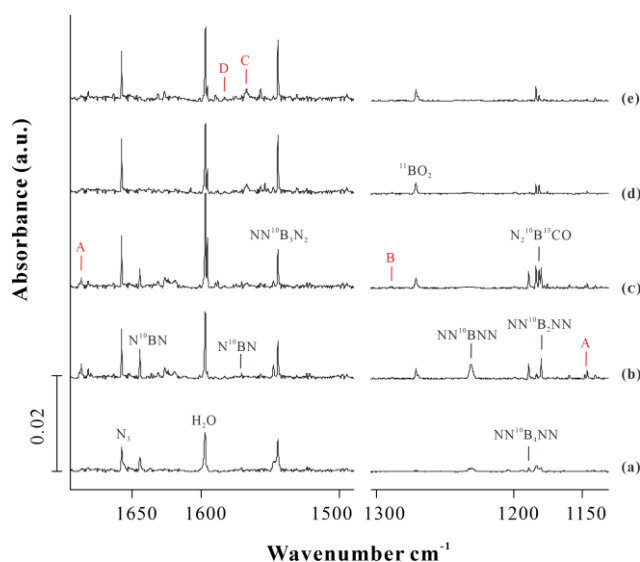


Fig. S4b. Infrared spectra in the 1700-1500 cm^{-1} , 1300-1150 cm^{-1} regions of laser-ablated ^{10}B -enriched boron atoms with 1% ^{13}CO in the N_2 matrix. (a) co-deposition at 4 K for 1 h; (b) after annealing to 25 K; (c) after 450 nm irradiation for 10 min; (d) after >220 nm irradiation for 10 min; (e) after annealing to 30 K. [A: NNBB CO , B: $(\eta^2\text{-N}_2)\text{BBCO}$, C: BNB NCO , D: BN CO].

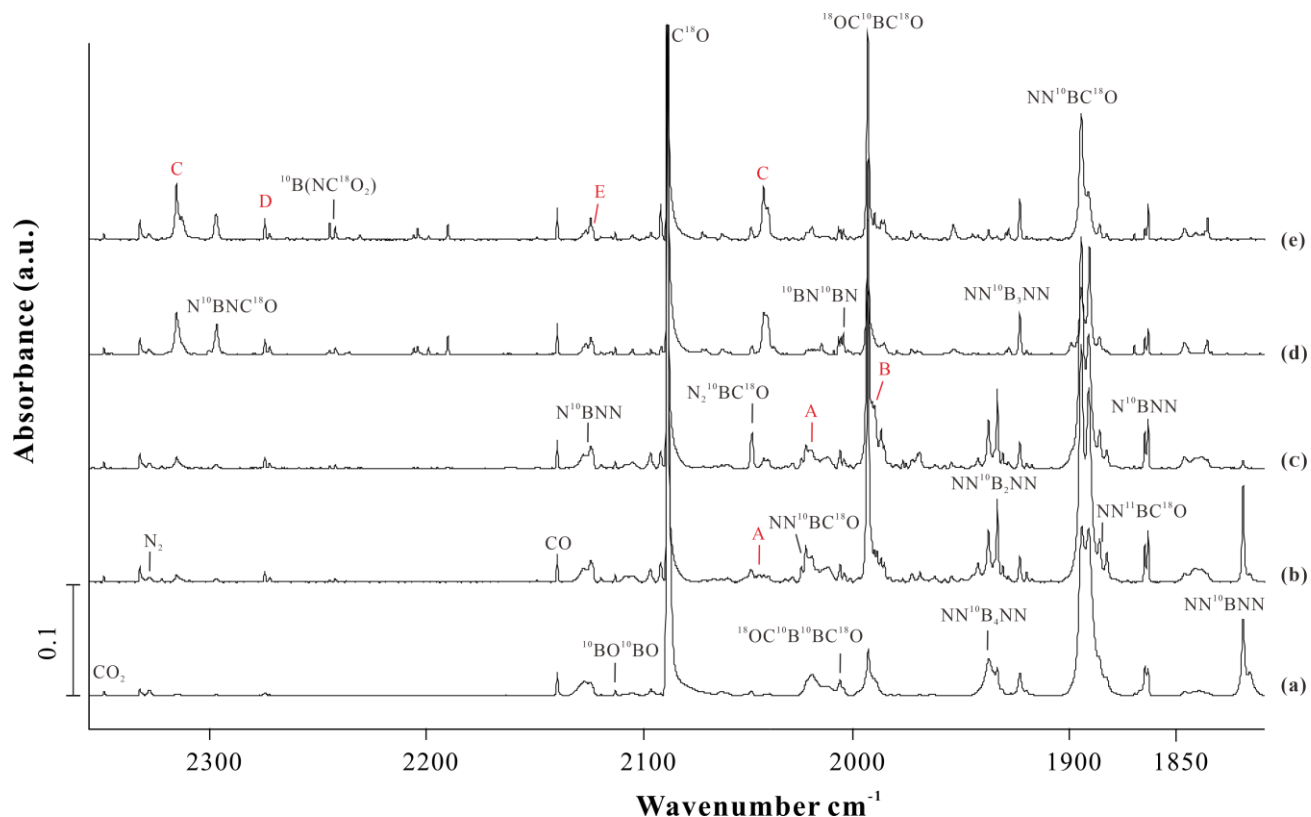


Fig. S5a. Infrared spectra in the 2350-1800 cm^{-1} region of laser-ablated ^{10}B -enriched boron atoms with 1% C^{18}O in the N_2 matrix. (a) co-deposition at 4 K for 1 h; (b) after annealing to 25 K; (c) after 450 nm irradiation for 10 min; (d) after >220 nm irradiation for 10 min; (e) after annealing to 30 K. [A: NNBBO, B: $(\eta^2\text{-N}_2)\text{BBCO}$, C: BNBNCO, D: BNCO, E: NBCO].

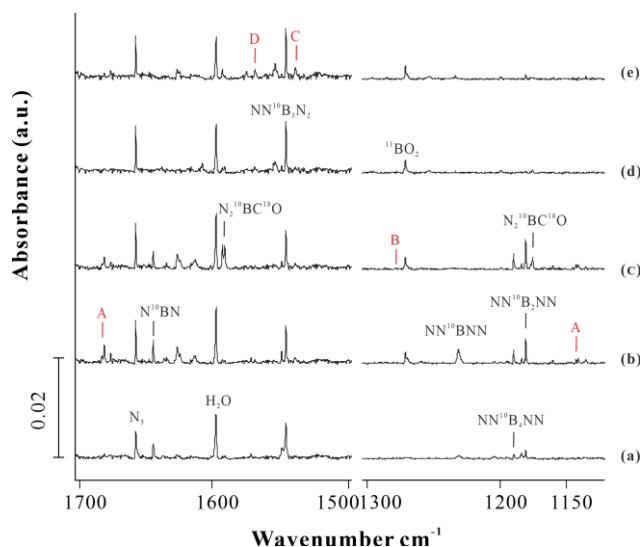
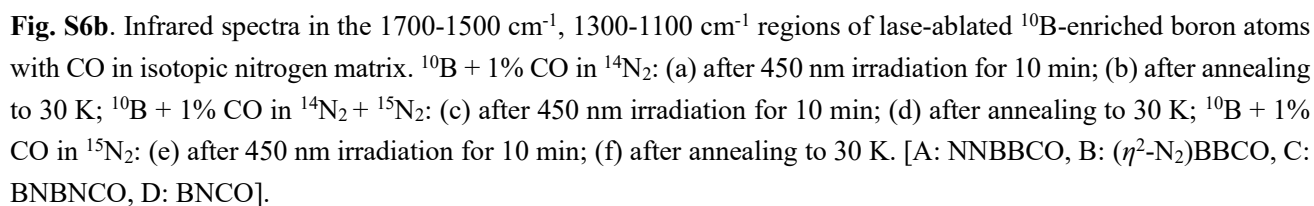
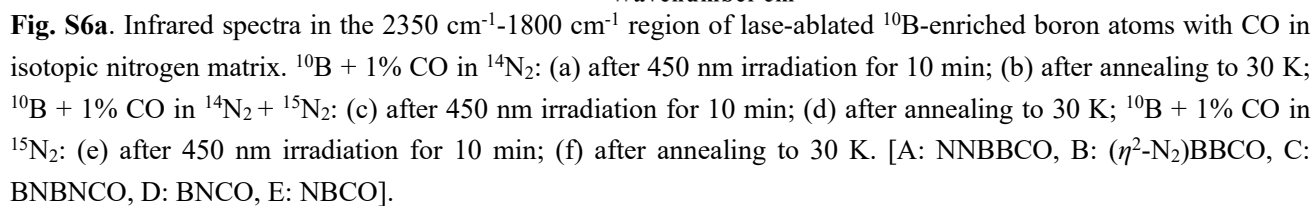


Fig. S5b. Infrared spectra in the 1700-1500 cm^{-1} , 1300-1100 cm^{-1} regions of laser-ablated ^{10}B -enriched boron atoms with 1% C^{18}O in the N_2 matrix. (a) co-deposition at 4 K for 1 h; (b) after annealing to 25 K; (c) after 450 nm irradiation for 10 min; (d) after >220 nm irradiation for 10 min; (e) after annealing to 30 K. [A: NNBBO, B: $(\eta^2\text{-N}_2)\text{BBCO}$, C: BNBNCO, D: BNCO].



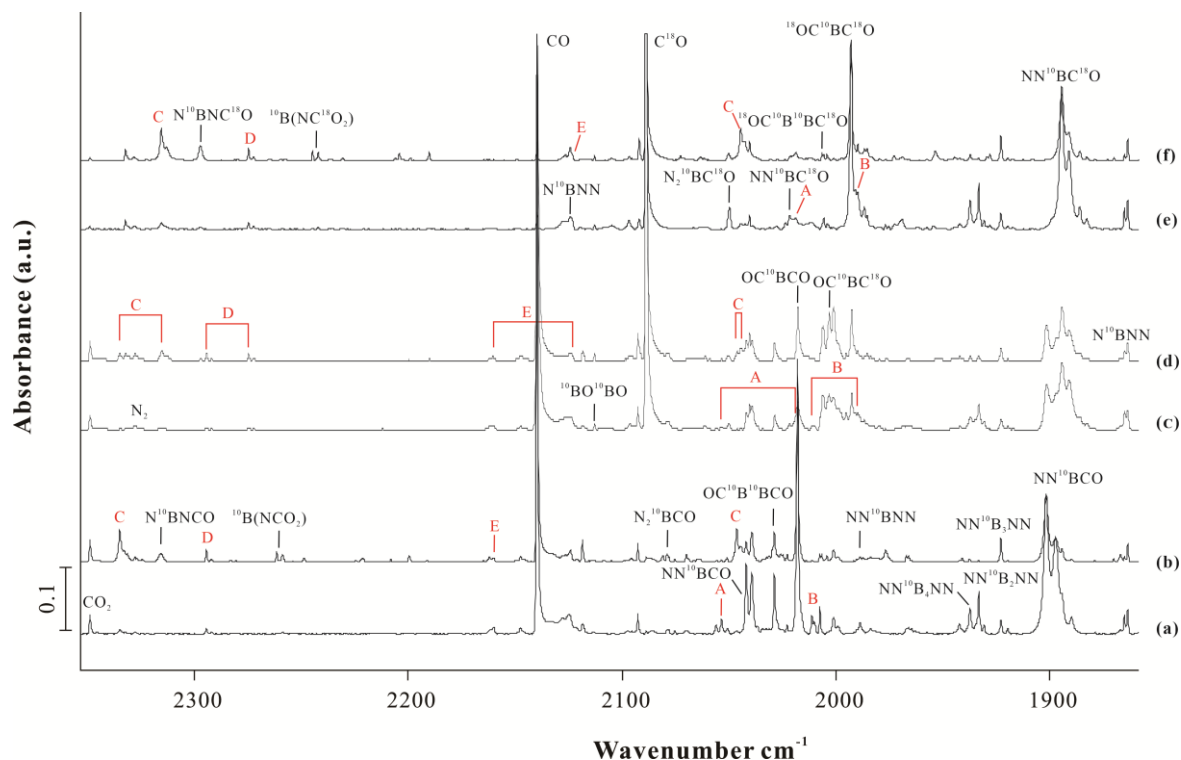


Fig. S8a. Infrared spectra in the 2350-1850 cm^{-1} region of lase-ablated ^{10}B -enriched boron atoms with $\text{CO}/\text{C}^{18}\text{O}$ in the N_2 matrix. $^{10}\text{B} + 1\% \text{CO}$ in $^{14}\text{N}_2$: (a) after 450 nm irradiation for 10 min; (b) after annealing to 30 K; $^{10}\text{B} + 1\% \text{CO} + 1\% \text{C}^{18}\text{O}$ in N_2 : (c) after 450 nm irradiation for 10 min; (d) after annealing to 30 K; $^{10}\text{B} + 1\% \text{C}^{18}\text{O}$ in N_2 : (e) after 450 nm irradiation for 10 min; (f) after annealing to 30 K. [A: NNBBCO, B: $(\eta^2\text{-N}_2)\text{BBCO}$, C: BNBNCO, D: BNCO, E: NBCO].

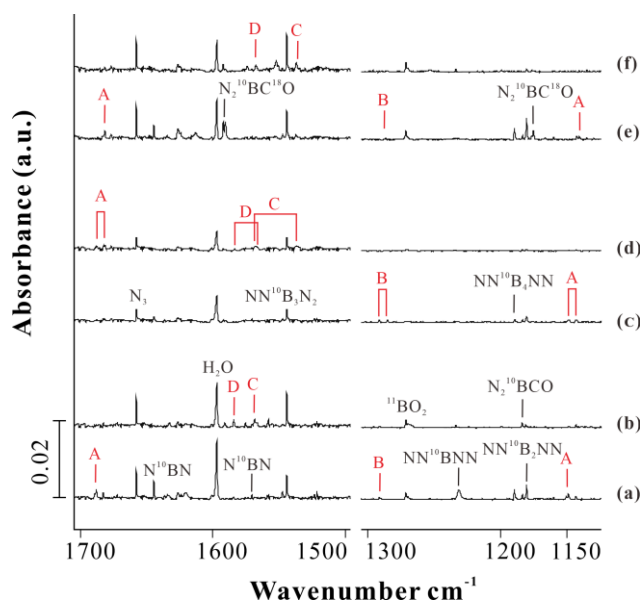


Fig. S8b. Infrared spectra in the 1700-1500 cm^{-1} , 1300-1100 cm^{-1} regions of lase-ablated ^{10}B -enriched boron atoms with $\text{CO}/\text{C}^{18}\text{O}$ in the N_2 matrix. $^{10}\text{B} + 1\% \text{CO}$ in $^{14}\text{N}_2$: (a) after 450 nm irradiation for 10 min; (b) after annealing to 30 K; $^{10}\text{B} + 1\% \text{CO} + 1\% \text{C}^{18}\text{O}$ in N_2 : (c) after 450 nm irradiation for 10 min; (d) after annealing to 30 K; $^{10}\text{B} + 1\% \text{C}^{18}\text{O}$ in N_2 : (e) after 450 nm irradiation for 10 min; (f) after annealing to 30 K. [A: NNBBCO, B: $(\eta^2\text{-N}_2)\text{BBCO}$, C: BNBNCO, D: BNCO].

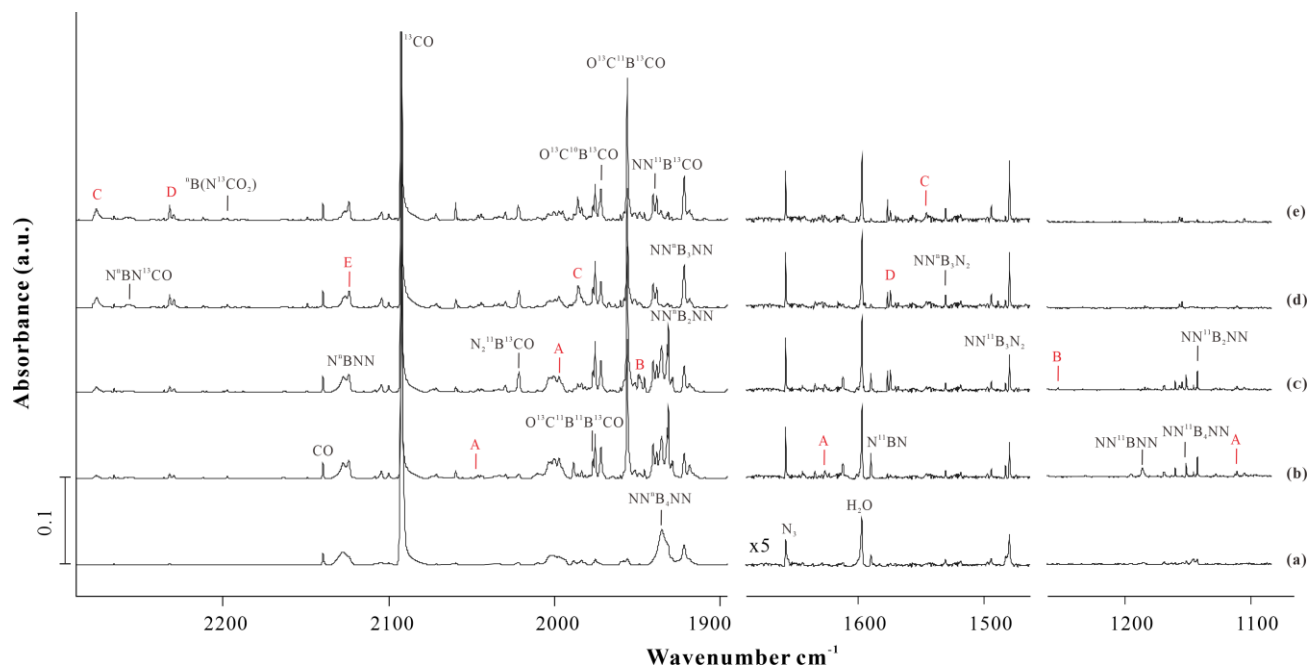


Fig. S9. Infrared spectra in the 2300-1900 cm^{-1} , 1650-1100 cm^{-1} regions of laser-ablated natural boron atoms with 1% ^{13}CO in the N_2 matrix. (a) co-deposition at 4 K for 1 h; (b) after annealing to 25 K; (c) after 450 nm irradiation for 10 min; (d) after >220 nm irradiation for 10 min; (e) after annealing to 30 K. [A: NNBBCO, B: ($\eta^2\text{-N}_2$)BBCO, C: BNBNCO, D: BNCO, E: NBCO].

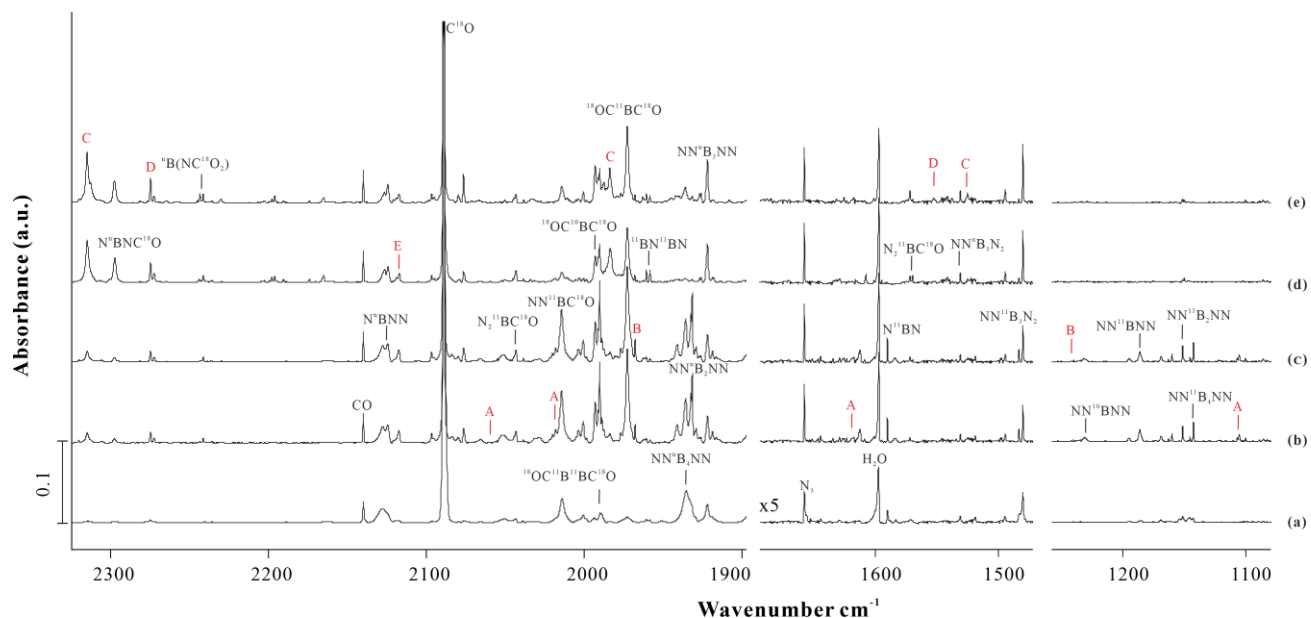


Fig. S10. Infrared spectra in the 2330-1900 cm^{-1} , 1650-1100 cm^{-1} regions of laser-ablated natural boron atoms with 1% C^{18}O in the N_2 matrix. (a) co-deposition at 4 K for 1 h; (b) after annealing to 25 K; (c) after 450 nm irradiation for 10 min; (d) after >220 nm irradiation for 10 min; (e) after annealing to 30 K. [A: NNBBCO, B: ($\eta^2\text{-N}_2$)BBCO, C: BNBNCO, D: BNCO, E: NBCO].

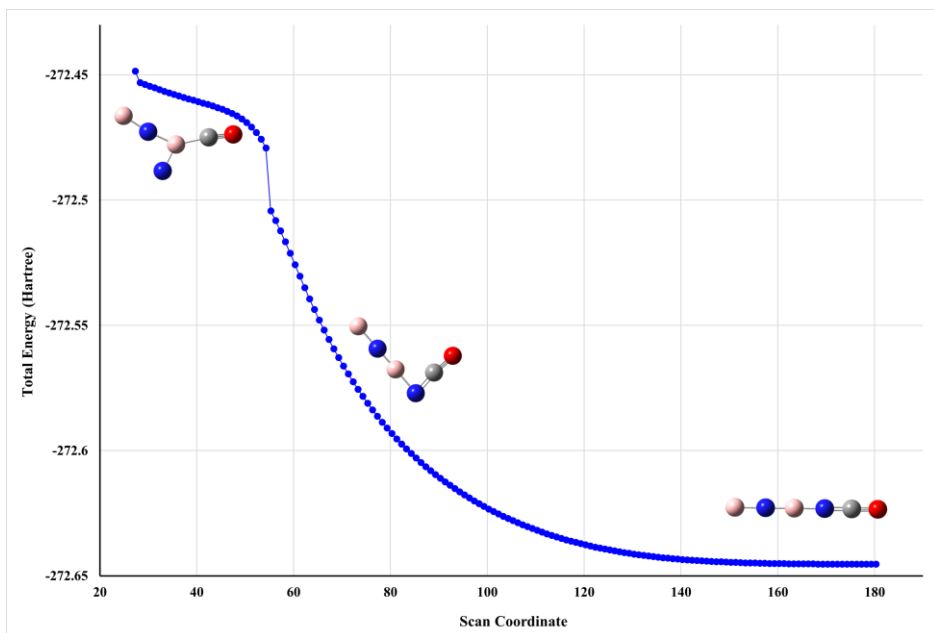


Fig. S11. Potential Energy Surface of BNBNCO from TS5 (in Fig. 3) at the B3LYP/def2-TZVPP level of theory.

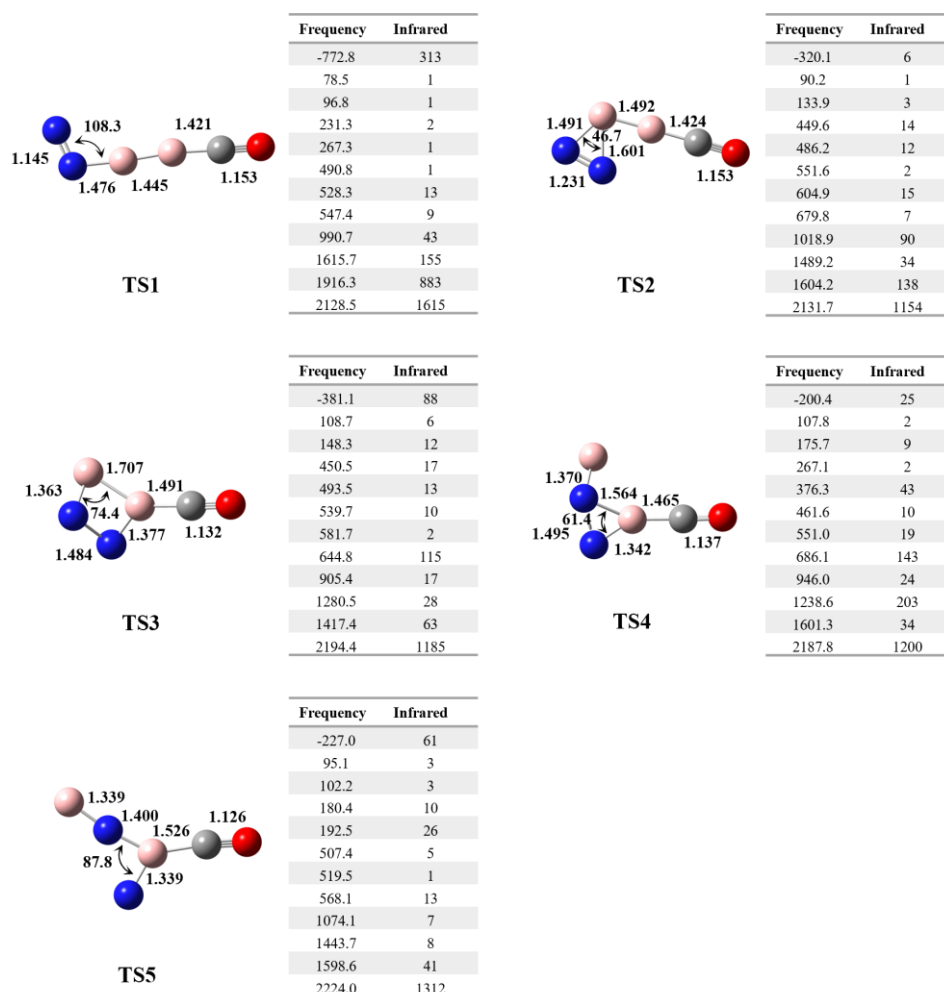


Fig. S12. Transition state structures (TS1-TS5) (1A_1 , C_1) (in Fig. 3) for the reaction from NNBBCO to (η^2-N_2) BBCO and BNBNCO and their frequencies (cm^{-1}) at the B3LYP/def2-TZVPP level of theory.

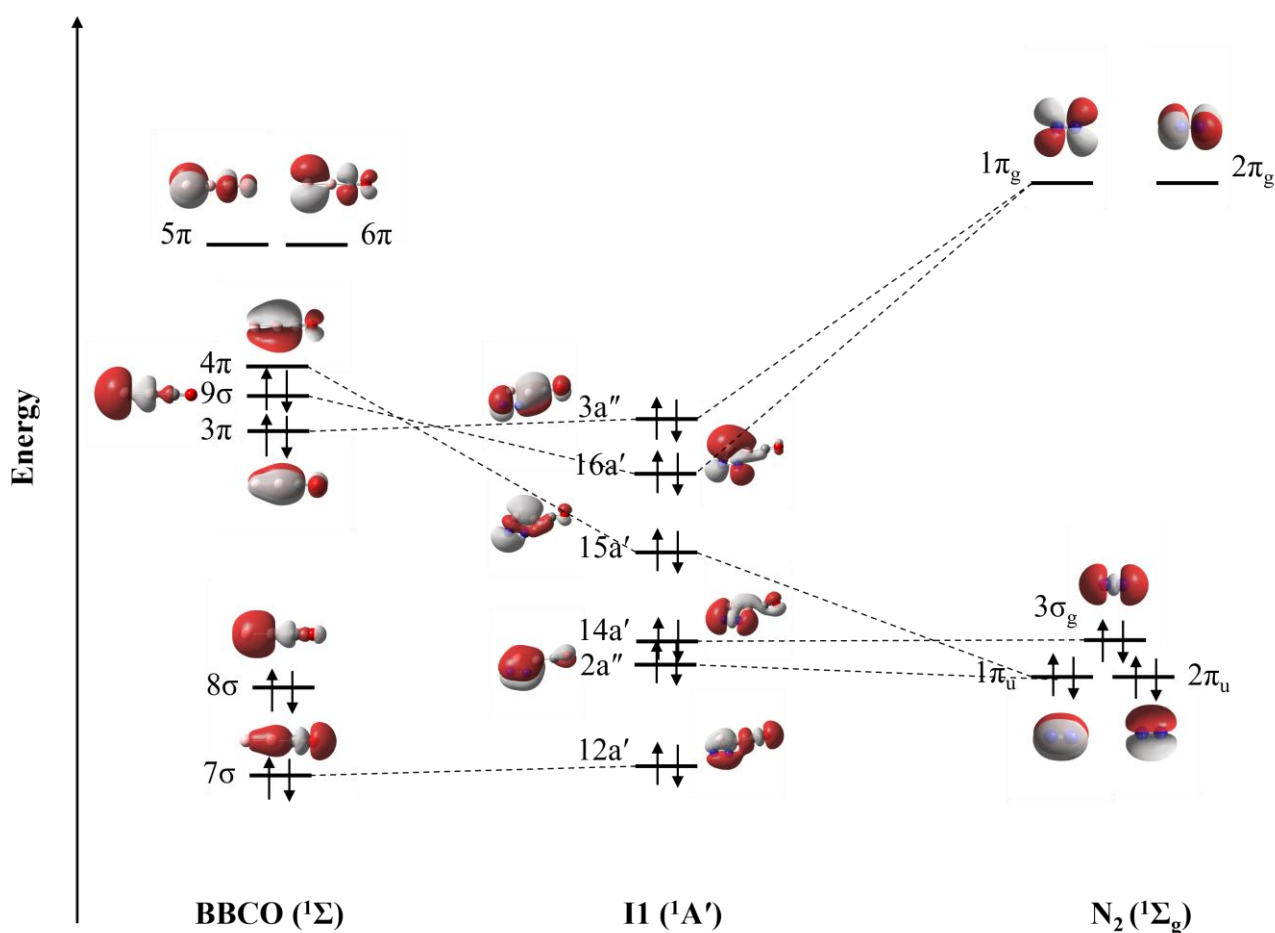


Fig. S13. Qualitative bonding scheme of the frontier molecular orbitals (FMOs, isovalue = 0.02 a.u.) of I1 ($^1A'$) (in Fig. 3) illustrating two fragments bonding interactions between a N₂ ($^1\Sigma_g$) molecule and a BBCO ($^1\Sigma$) fragment which were optimized at the B3LYP/def2-TZVPP level.

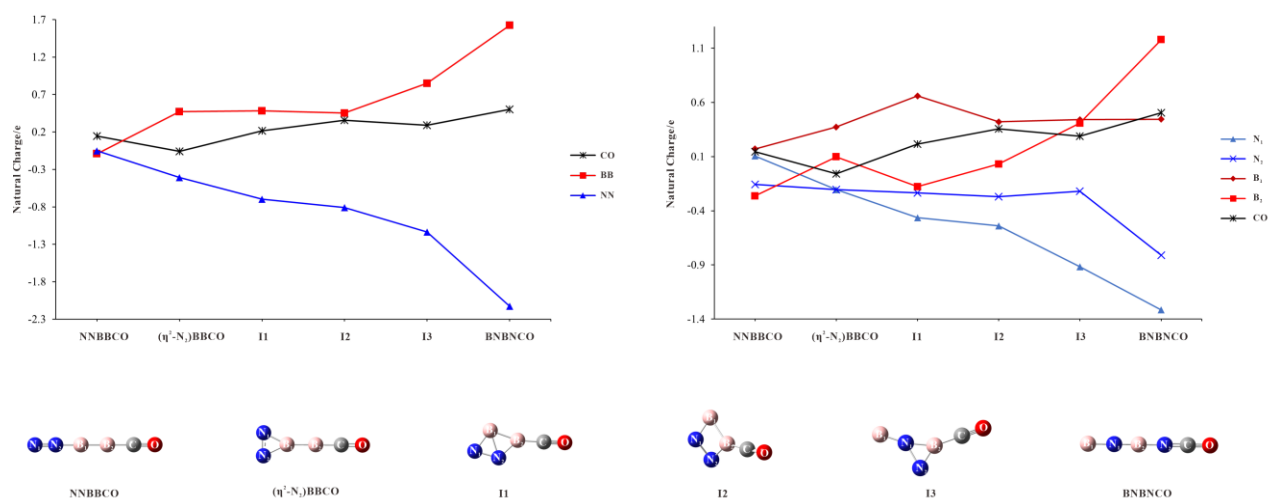


Fig. S14. Charges on atoms of stationary points along the isomerization process of NNBBCO to BNBNCO.

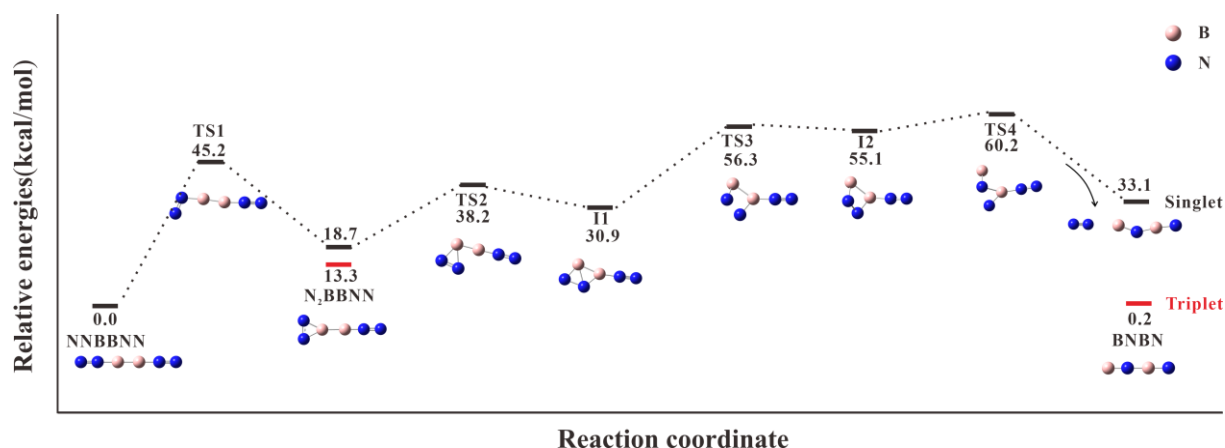


Fig. S15. Potential energy surface for the reaction from NNBBNN to $(\eta^2\text{-N}_2)\text{BBNN}$ and $\text{BNNB} + \text{N}_2$ calculated at the B3LYP/def2-TZVPP level. Energies were given in kcal/mol. Red lines denote stationary points on the triplet surface and black lines on the singlet surface.

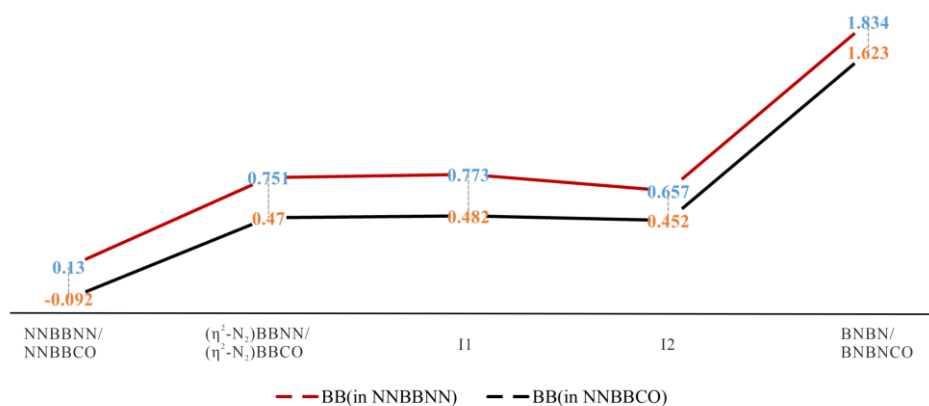


Fig. S16. Charges on B–B centres of stationary points along the isomerization process of NNBBNN or NNBBCO.

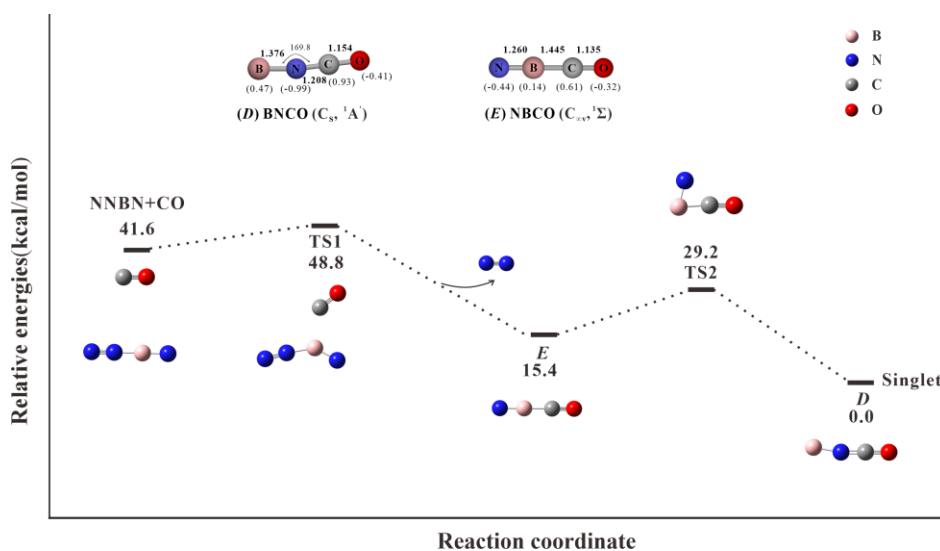


Fig. S17. Potential energy surface for the reaction of NNBN with CO to form NBCO (*E*) and BNCO (*D*) calculated at the B3LYP/def2-TZVPP level. Energies were given in kcal/mol. Top: Structures of the BNCO (*D*) and NBCO (*E*) optimized at the B3LYP/def2-TZVPP functionals/basis set. Bond lengths were in Å and angles in degree. The natural population charges were given in parentheses.

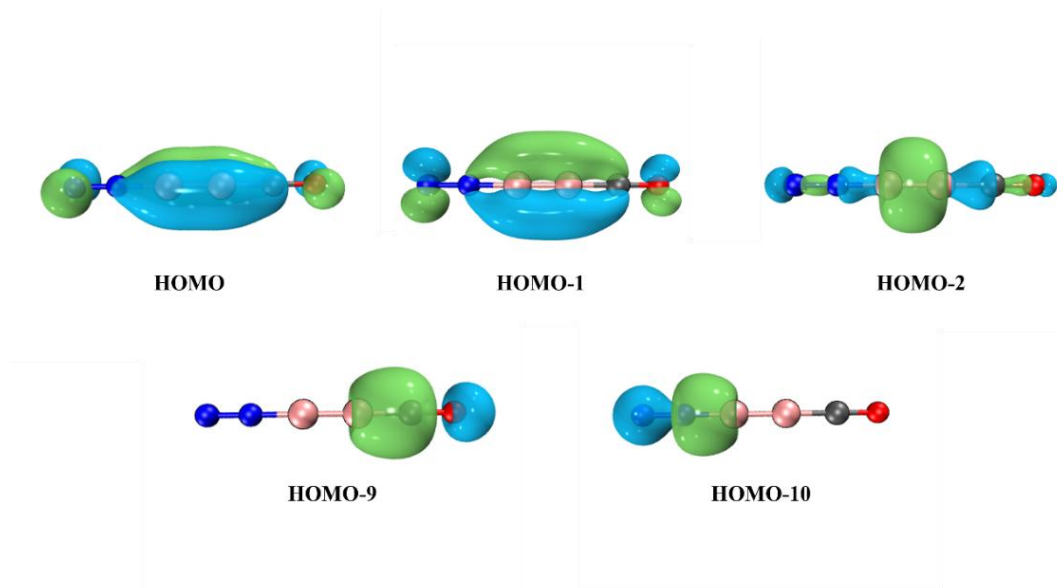


Fig. S18. Selected frontier molecular orbitals of NNBBCO (*A*) ($C_{\infty v}, {}^1\Sigma$) calculated at the B3LYP/def2-TZVPP level.

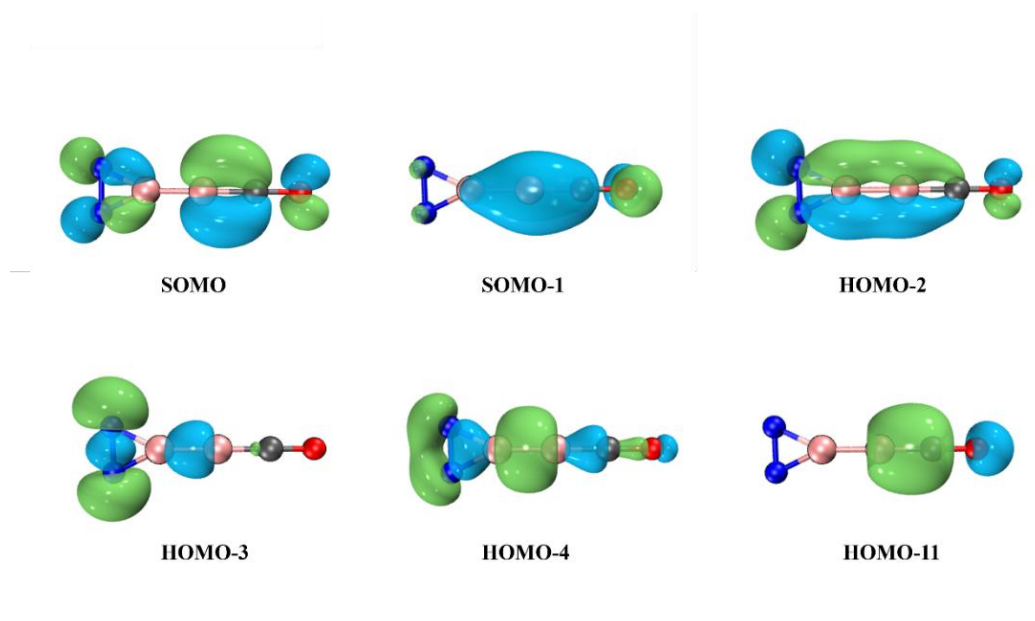


Fig. S19. Selected frontier molecular orbitals of $(\eta^2\text{-N}_2)\text{BBCO}$ (*B*) ($C_{2v}, {}^3A_2$) calculated at the B3LYP/def2-TZVPP level.

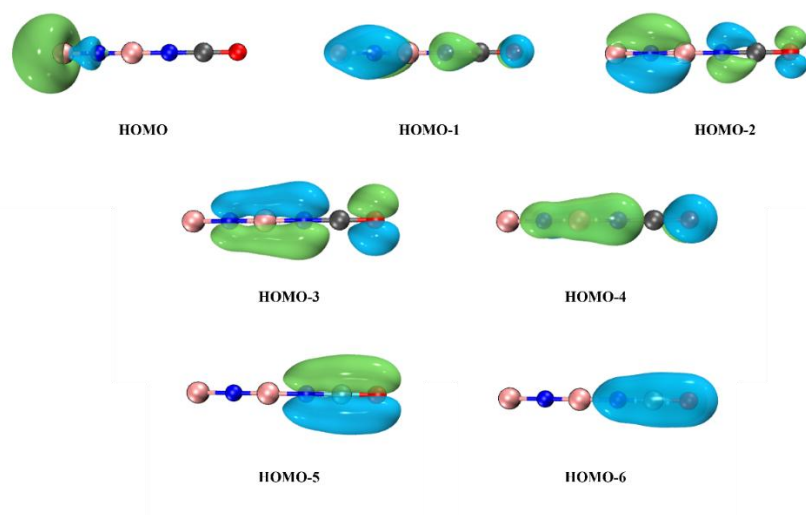


Fig. S20. Selected frontier molecular orbitals of BNBNC(O) (C) ($C_{\infty v}$, $^1\Sigma$) calculated at the B3LYP/def2-TZVPP level.

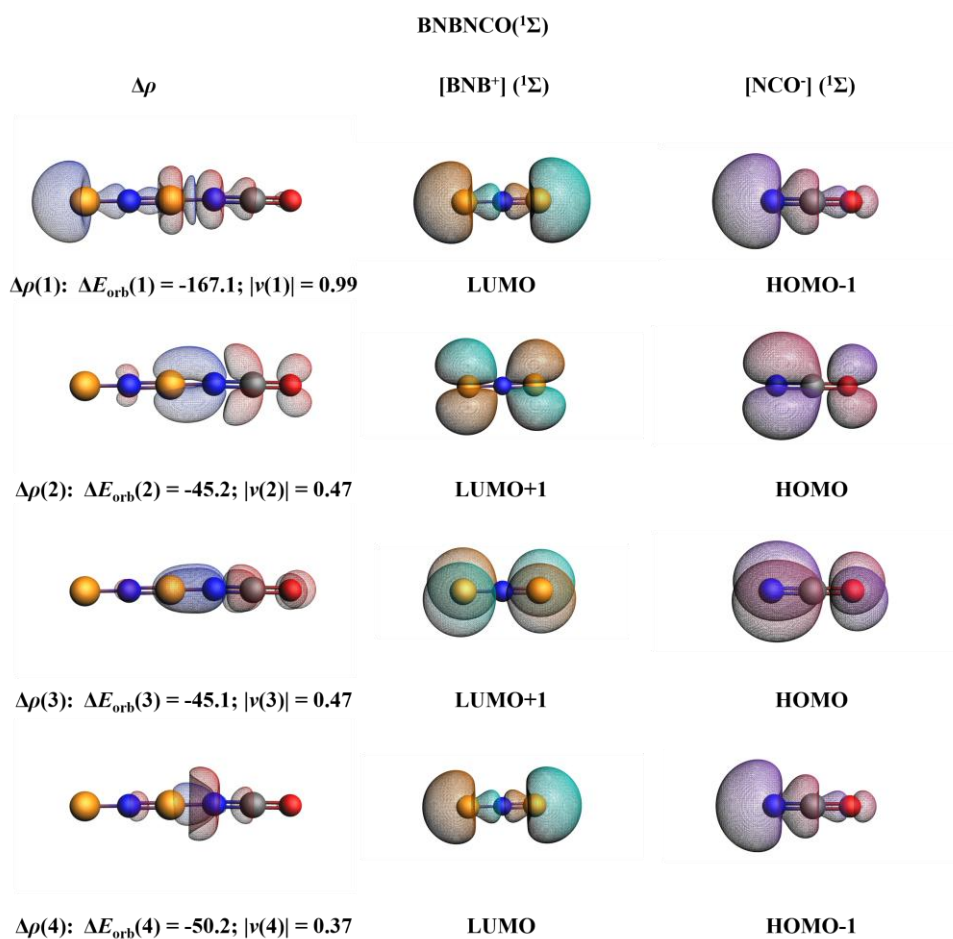


Fig. S21. Plot of the deformation densities $\Delta\rho$ of BNBNC(O) ($^1\Sigma$) at the Hybrid/B3LYP/TZ2P level taking [BNB $^+$] ($^1\Sigma$) and [NCO $^-$] ($^1\Sigma$) as interacting fragments with the associated interaction energy ΔE_{orb} (in kcal/mol) and charge eigenvalues $|v_n|$ (in e). Isosurface value is 0.003 a.u. The color coding of the deformation densities $\Delta\rho(n)$ gives the charge flow from the red to the blue area.

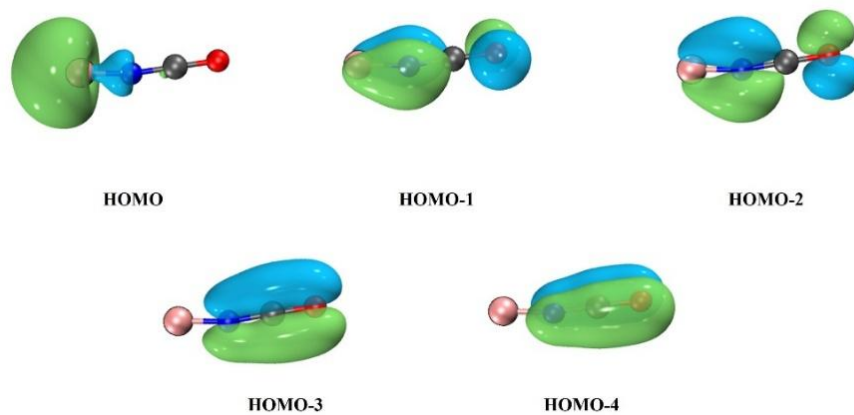


Fig. S22. Selected frontier molecular orbitals of BNCO (*D*) (C_s , $^1A'$) calculated at the B3LYP/def2-TZVPP level.

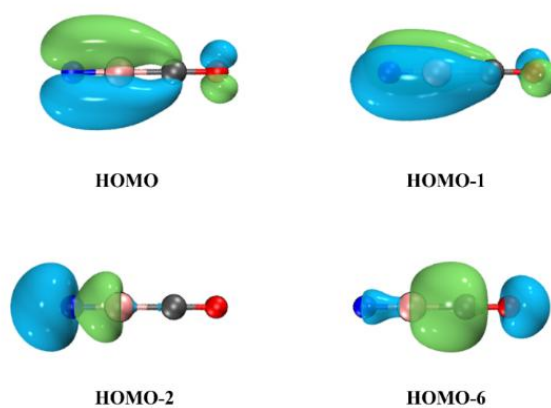


Fig. S23. Selected frontier molecular orbitals of NBCO (*E*) ($C_{\infty v}$, $^1\Sigma$) calculated at the B3LYP/def2-TZVPP level.

Supplementary Tables

Table S1. Observed and calculated (B3LYP/def2-TZVPP) infrared absorptions (cm^{-1}) and intensities (km/mol, in parentheses) for isotopomers of products *A-E* in the reactions of ^{10}B with CO in a N_2 matrix.

	Assignment	$^{10}\text{B}+\text{CO}/^{14}\text{N}_2$		$^{10}\text{B}+^{13}\text{CO}/^{14}\text{N}_2$		$^{10}\text{B}+\text{C}^{18}\text{O}/^{14}\text{N}_2$		$^{10}\text{B}+\text{CO}/^{15}\text{N}_2$	
		B3LYP ^[a]	Obs.	B3LYP ^[a]	Obs.	B3LYP ^[a]	Obs.	B3LYP ^[a]	Obs.
(A) NNBBCO ($^1\Sigma$)	NN, CO sym	2081.4 (133)	2066.5	2071.7 (498)	2053.2	2072.8 (307)	2046.5	2074.3 (1354)	2050.2
	NN, CO asym	2061.3 (2507)	2053.6	2020.0 (2035)	1999.8	2037.1 (2266)	2018.7	1999.0 (1225)	1990.1
	BB str	1746.6 (44)	1688.0	1745.5 (57)	1687.0	1739.9 (71)	1681.6	1745.2 (37)	1686.4
	BB str	1117.8 (78)	1149.0	1117.1 (80)	1147.1	1109.5 (70)	1140.8	1112.4 (76)	1143.7
(B) ($\eta^2\text{-N}_2$)BBCO ($^3\text{A}_2$)	CO str	2001.2 (854)	2011.2	1949.8 (812)	1967.3	1970.8 (819)	1989.7	2001.2 (853)	2009.5
	NN str	1623.8 (36)	/	1623.7 (35)	/	1622.5 (33)	/	1596.0 (26)	/
	BB str	1323.7 (80)	1291.3	1323.7 (80)	1289.7	1312.5 (89)	1279.1	1311.5 (80)	1280.8
(C) BNBBCO ($^1\Sigma$)	CO str	2356.4 (2228)	2335.1	2294.8 (2236)	2276.9	2341.1 (2254)	2315.6	2341.2 (2116)	2322.7
	BN str	2046.8 (2147)	2046.3	2045.6 (2033)	2045.9	2044.8 (2092)	2044.4	2022.5 (2143)	2021.3
	BN str	1576.3 (211)	1568.7	1574.2 (221)	1567.0	1556.7 (224)	1537.5	1541.9 (200)	1536.5
	BN str	1235.5 (109)	/	1235.4 (110)	/	1223.4 (97)	/	1227.0 (119)	/
(D) BNCO (^1A)	CO str	2306.7 (1540)	2294.5	2244.1 (1496)	2232.4	2288.4 (1543)	2274.8	2295.1 (1480)	2285.3
	BN str	1586.1 (280)	1584.4	1584.7 (267)	1583.1	1563.2 (266)	1567.7	1555.5 (295)	1550.6
	BN str	921.5 (131)	/	919.6 (129)	/	905.6 (125)	/	920.7 (129)	/
(E) NBCO ($^1\Sigma$)	CO str	2174.4 (1008)	2160.2	2125.1 (970)	2108.4	2141.7 (1000)	2123.3	2173.2 (1004)	2160.0
	BN str	1939.3 (12)	/	1935.1 (3)	/	1928.1 (1)	/	1921.4 (17)	/

[a] Scaled frequencies using a scaling factor of 0.9661, which is obtained from the ratio of the experimental stretching frequency (2139 cm^{-1}) and the calculated value (2214 cm^{-1}) for CO.

Table S2. Comparisons between experimental and calculated vibrational frequencies and isotopic frequency ratios of products *A-E* in the reactions of boron with CO in a N₂ matrix.

				¹⁰ B/ ¹¹ B		¹² C/ ¹³ C		¹⁶ O/ ¹⁸ O		¹⁴ N/ ¹⁵ N	
	Assignment	B3LYP ^[a]	Obs.	Cal.	Exp.	Cal.	Exp.	Cal.	Exp.	Cal.	Exp.
(A) NNBBCO (¹ Σ)	NN, CO sym	2081.4	2066.5	1.0019	/	1.0047	1.0065	1.0041	1.0098	1.0034	1.0080
	NN, CO asym	2061.3	2053.6	1.0015	1.0030	1.0204	1.0269	1.0119	1.0173	1.0312	1.0319
	BB str	1746.6	1688.0	1.0442	1.0377	1.0007	1.0006	1.0038	1.0038	1.0008	1.0009
	BB str	1117.8	1149.0	1.0342	1.0318	1.0006	1.0017	1.0075	1.0072	1.0049	1.0046
(B) (η ² -N ₂)BBCO (³ A ₂)	CO str	2001.2	2011.2	1.0027	1.0070	1.0264	1.0223	1.0154	1.0108	1.0000	1.0008
	NN str	1623.8	/	1.0201	/	1.0000	/	1.0008	/	1.0174	/
	BB str	1323.7	1291.3	1.0301	1.0303	1.0000	1.0012	1.0085	1.0095	1.0093	1.0082
(C) BNBNCO (¹ Σ)	CO str	2356.4	2335.1	1.0002	1.0004	1.0269	1.0256	1.0066	1.0084	1.0065	1.0053
	BN str	2046.8	2046.3	1.0290	1.0301	1.0006	1.0002	1.0009	1.0009	1.0120	1.0124
	BN str	1576.3	1568.7	1.0046	1.0139	1.0014	1.0011	1.0126	1.0203	1.0223	1.0210
	BN str	1235.5	/	1.0315	/	1.0002	/	1.0100	/	1.0069	/
(D) BNCO (¹ A')	CO str	2306.7	2294.5	1.0001	1.0001	1.0279	1.0278	1.0080	1.0087	1.0050	1.0040
	BN str	1586.1	1584.4	1.0073	1.0049	1.0008	1.0008	1.0146	1.0107	1.0197	1.0218
	BN str	921.5	/	1.0308	/	1.0021	/	1.0176	/	1.0009	/
(E) NBCO (¹ Σ)	CO str	2174.4	2160.2	1.0041	1.0017	1.0232	1.0246	1.0152	1.0174	1.0005	1.0001
	BN str	1939.3	/	1.0290	/	1.0022	/	1.0058	/	1.0094	/

[a] Scaled frequencies using a scaling factor of 0.9661, which is obtained from the ratio of the experimental stretching frequency (2139 cm⁻¹) and the calculated value (2214 cm⁻¹) for CO.

Table S3. Observed and calculated (B3LYP/def2-TZVPP) infrared absorptions (cm^{-1}) and intensities (km/mol , in parentheses) for isotopomers of products **A-E** in the reactions of ^{10}B with CO in a N_2 matrix.

	Assignment	$^{11}\text{B}^{11}\text{B}$		$^{10}\text{B}^{11}\text{B}$		$^{11}\text{B}^{10}\text{B}$		$^{10}\text{B}^{10}\text{B}$	
		B3LYP ^[a]	Obs.	B3LYP ^[a]	Obs.	B3LYP ^[a]	Obs.	B3LYP ^[a]	Obs.
(A) NNBBCO ($^1\Sigma$)	NN, CO sym	2077.4 (24)	/	2078.7 (19)	/	2079.9 (151)	2065.3	2081.4 (133)	2066.5
	NN, CO asym	2058.3 (2616)	2047.5	2058.4 (2622)	2047.5	2061.3 (2491)	2053.6	2061.3 (2507)	2053.6
	BB str	1672.6 (25)	1626.7	1713.6 (32)	1643.1	1708.5 (34)	1634.6	1746.6 (44)	1688.0
	BB str	1080.8 (77)	1113.6	1097.4 (77)	1131.5	1098.6 (78)	1129.7	1117.8 (78)	1149.0
(B) ($\eta^2\text{-N}_2$)BBCO ($^3\text{A}_2$)	CO str	1995.8 (812)	1997.2	1995.8 (855)	1997.2	2001.2 (853)	2011.2	2001.2 (854)	2011.2
	NN str	1591.8 (52)	/	1617.3 (46)	/	1598.1 (41)	/	1623.8 (36)	/
	BB str	1285.0 (65)	1253.3	1287.7 (70)	1257.3	1322.6 (76)	1290.4	1323.7 (80)	1291.3
(C) BNBBCO ($^1\Sigma$)	CO str	2356.0 (2186)	2334.1	2356.1 (2177)	2334.1	2356.3 (2237)	2334.1	2347.7 (2228)	2335.1
	BN str	1989.0 (2095)	1986.5	1990.7 (2130)	1988.6	2045.4 (2115)	2044.7	2046.8 (2147)	2046.3
	BN str	1569.1 (188)	1547.2	1575.9 (197)	1567.0	1569.3 (197)	1548.5	1576.3 (211)	1568.7
	BN str	1197.8 (91)	/	1221.5 (89)	/	1211.8 (111)	/	1235.5 (109)	/
(D) BNCO ($^1\text{A}'$)	CO str	2306.5 (1534)	2294.3	/	/	/	/	2306.7 (1540)	2294.5
	BN str	1574.5 (261)	1576.7	/	/	/	/	1586.0 (280)	1584.4
	BN str	894.0 (129)	/	/	/	/	/	921.5 (131)	/
(E) NBCO ($^1\Sigma$)	CO str	2165.6 (970)	2156.5					2174.4 (1008)	2160.2
	BN str	1884.7 (13)	/					1939.3 (12)	/

[a] Scaled frequencies using a scaling factor of 0.9661, which is obtained from the ratio of the experimental stretching frequency (2139 cm^{-1}) and the calculated value (2214 cm^{-1}) for CO.

Table S4. Observed and calculated (B3LYP/def2-TZVPP) infrared absorptions (cm^{-1}) and intensities (km/mol , in parentheses) for isotopomers of products *A-E* in the reactions of ^{10}B with CO in a N_2 matrix.

		$^{11}\text{B}+^{14}\text{CO}/^{14}\text{N}_2$		$^{11}\text{B}+^{13}\text{CO}/^{14}\text{N}_2$		$^{11}\text{B}+^{18}\text{O}/^{14}\text{N}_2$	
	Assignment	B3LYP ^[a]	Obs.	B3LYP ^[a]	Obs.	B3LYP ^[a]	Obs.
(A) NNBBCO ($^1\Sigma$)	NN, CO sym	2077.4 (24)	/	2070.4 (549)	2048.0	2071.1 (403)	2046.2
	NN, CO asym	2058.3 (2616)	2047.5	2013.4 (1992)	1997.5	2030.1 (2181)	2018.1
	BB str	1672.6 (25)	1626.7	1672.2 (29)	1626.5	1667.5 (39)	1618.8
	BB str	1080.8 (77)	1113.6	1080.0 (79)	1111.2	1072.6 (69)	1106.6
(B) ($\eta^2\text{-N}_2$)BBCO ($^3\text{A}_2$)	CO str	1995.8 (812)	1997.2	1944.2 (812)	1949.5	1964.5 (819)	1970.2
	NN str	1591.8 (52)	/	1591.8 (51)	/	1591.1 (49)	/
	BB str	1285.0 (65)	1253.3	1285.0 (64)	1253.3	1274.3 (73)	1242.4
(C) BNBBCO ($^1\Sigma$)	CO str	2356.0 (2186)	2334.1	2294.3 (2160)	2276.4	2340.7 (2200)	2314.8
	BN str	1989.0 (2095)	1986.5	1988.0 (2016)	1986.0	1987.0 (2054)	1983.8
	BN str	1569.1 (188)	1547.2	1567.0 (197)	1545.8	1548.4 (195)	1525.1
	BN str	1197.8 (91)	/	1197.6 (93)	/	1186.8 (83)	/
(D) BNCO ($^1\text{A}'$)	CO str	2306.5 (1534)	2294.3	2243.9 (1489)	2232.4	2288.2 (1563)	2274.5
	BN str	1574.5 (261)	1576.7	1573.3 (249)	1575.7	1550.8 (247)	1552.4
	BN str	894.0 (129)	/	891.9 (127)	/	878.8 (123)	/
(E) NBCO ($^1\Sigma$)	CO str	2165.6 (970)	2156.5	2113.9 (932)	2104.3	2129.5 (967)	2117.0
	BN str	1884.7 (13)	/	1882.8 (22)	/	1877.0 (13)	/

[a] Scaled frequencies using a scaling factor of 0.9661, which is obtained from the ratio of the experimental stretching frequency (2139 cm^{-1}) and the calculated value (2214 cm^{-1}) for CO.

Table S5. Comparisons between experimental and calculated vibrational frequencies and isotopic frequency ratios of products *A-E* in the reactions of ^{11}B with CO in a $^{14}\text{N}_2$ matrix.

	Assignment	$^{11}\text{B}+\text{CO}/^{14}\text{N}_2$		$^{12}\text{C}/^{13}\text{C}$		$^{16}\text{O}/^{18}\text{O}$	
		B3LYP ^[a]	Obs.	Cal.	Exp.	Cal.	Exp.
(A) NNBBCO ($^1\Sigma$)	NN, CO sym	2077.4	/	1.0034	/	1.0030	/
	NN, CO asym	2058.3	2047.5	1.0223	1.0250	1.0139	1.0146
	BB str	1672.6	1626.7	1.0002	1.0001	1.0031	1.0049
	BB str	1080.8	1113.6	1.0007	1.0022	1.0077	1.0063
(B) ($\eta^2\text{-N}_2$)BBCO ($^3\text{A}_2$)	CO str	1995.8	1997.2	1.0265	1.0245	1.0159	1.0137
	NN str	1591.8	/	1.0000	/	1.0005	/
	BB str	1285.0	1253.3	1.0000	1.0000	1.0084	1.0088
(C) BNBNC O ($^1\Sigma$)	CO str	2356.0	2334.1	1.0269	1.0253	1.0066	1.0083
	BN str	1989.0	1986.5	1.0005	1.0003	1.0010	1.0014
	BN str	1569.1	1547.2	1.0014	1.0009	1.0134	1.0145
	BN str	1197.8	/	1.0002	/	1.0093	/
(D) BNCO ($^1\text{A}'$)	CO str	2306.5	2294.3	1.0279	1.0277	1.0080	1.0087
	BN str	1574.5	1576.7	1.0008	1.0006	1.0153	1.0157
	BN str	894.0	/	1.0023		1.0173	
(E) NBCO ($^1\Sigma$)	CO str	2165.6	2156.5	1.0245	1.0248	1.0170	1.0187
	BN str	1884.7	/	1.0010	/	1.0041	/

[a] Scaled frequencies using a scaling factor of 0.9661, which is obtained from the ratio of the experimental stretching frequency (2139 cm^{-1}) and the calculated value (2214 cm^{-1}) for CO.

Table S6. Orbital composition analysis on the II ($^1A'$) complex by Natural Atomic Orbital (NAO) method.

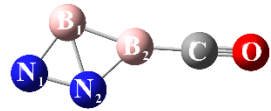
Complex	Orbital	Composition
 <p>II</p>	HOMO (3a'')	$N_1\ 2p_z\ (34\%) + N_2\ 2p_z\ (3\%) + B_2\ 2p_z\ (37\%) + C\ 2p_z\ (13\%) + O\ 2p_z\ (12\%)$
	HOMO-1 (16a')	$N_1\ 2s\ (5\%) + 2p_x\ (4\%) + 2p_y\ (17\%) + N_2\ 2s\ (3\%) + 2p_y\ (27\%) + B_1\ 2s\ (23\%) + 2p_x\ (4\%) + 2p_y\ (10\%) + B_2\ 2p_y\ (4\%)$
	HOMO-2 (15a')	$N_1\ 2s\ (5\%) + 2p_x\ (7\%) + 2p_y\ (29\%) + B_1\ 2s\ (8\%) + 2p_x\ (8\%) + 2p_y\ (9\%) + B_2\ 2s\ (7\%) + 2p_x\ (11\%) + 2p_y\ (11\%) + O\ 2p_z\ (2\%)$
	HOMO-3 (2a'')	$N_1\ 2s\ (15\%) + 2p_x\ (28\%) + N_2\ 2s\ (2\%) + 2p_x\ (27\%) + 2p_y\ (4\%) + B_1\ 2p_x\ (7\%) + B_2\ 2p_y\ (8\%) + N_2\ 2p_y\ (39\%) + O\ 2p_y\ (4\%)$
	HOMO-4 (1a'')	$N_1\ 2p_z\ (28\%) + N_2\ 2p_z\ (49\%) + B_1\ 2p_z\ (10\%) + B_2\ 2p_z\ (7\%) + O\ 2p_z\ (5\%)$
	HOMO-5 (14a')	$N_2\ 2p_z\ (2\%) + B_2\ 2p_z\ (3\%) + C\ 2p_z\ (30\%) + O\ 2p_z\ (63\%)$
	HOMO-6 (13a')	$N_1\ 2p_x\ (1\%) + B_2\ 2p_y\ (2\%) + C\ 2p_y\ (29\%) + O\ 2p_y\ (62\%)$
	HOMO-7 (12a')	$N_1\ 2p_y\ (9\%) + N_2\ 2s\ (4\%) + 2p_y\ (14\%) + B_1\ 2s\ (3\%) + B_2\ 2p_x\ (10\%) + C\ 2p_x\ (9\%) + O\ 2s\ (9\%) + 2p_x\ (37\%)$
	HOMO-8 (11a')	$N_1\ 2p_x\ (4\%) + 2p_y\ (15\%) + N_2\ 2s\ (10\%) + 2p_y\ (19\%) + B_1\ 2s\ (10\%) + B_2\ 2s\ (3\%) + 2p_y\ (2\%) + C\ 2p_x\ (4\%) + O\ 2s\ (6\%) + 2p_x\ (21\%) + 2p_y\ (2\%)$
	HOMO-9 (10a')	$N_1\ 2s\ (5\%) + N_2\ 2s\ (3\%) + B_2\ 2s\ (5\%) + 2p_x\ (19\%) + 2p_y\ (2\%) + C\ 2s\ (28\%) + 2p_x\ (15\%) + O\ 2s\ (7\%) + 2p_x\ (11\%)$
	HOMO-10 (9a')	$N_1\ 2s\ (24\%) + N_2\ 2s\ (14\%) + 2p_x\ (23\%) + 2p_y\ (5\%) + B_1\ 2p_x\ (7\%) + B_2\ 2s\ (12\%) + 2p_y\ (3\%) + C\ 2s\ (4\%) + 2p_x\ (4\%)$
	HOMO-11 (8a')	$N_1\ 2s\ (24\%) + 2p_x\ (10\%) + N_2\ 2s\ (35\%) + 2p_x\ (6\%) + 2p_y\ (3\%) + B_1\ 2s\ (5\%) + 2p_y\ (5\%) + B_2\ 2s\ (3\%) + 2p_x\ (3\%) + 2p_y\ (2\%)$

Table S7. EDA-NOCV results of I1 ($^1A'$) at the Hybrid/B3LYP/TZ2P level taking BBCO ($^1A'$) and N_2 ($^1\Sigma_g$) as interacting fragments. Energy values are in kcal/mol.

Energy terms	Orbital interaction	I1 ($^1A'$) BBCO ($^1A'$) + N_2 ($^1\Sigma_g$)
ΔE_{int}		-114.4
ΔE_{Pauli}		740.6
$\Delta E_{\text{elstat}}^{[a]}$		-283.2 (33.1%)
$\Delta E_{\text{orb}}^{[a]}$		-571.8 (66.9%)
$\Delta E_{\text{orb}}(1)^{[b]}$	BBCO HOMO (10a') \rightarrow N_2 LUMO ($2\pi_g$) donation	-305.5 (53.4%)
$\Delta E_{\text{orb}}(2)^{[b]}$	BBCO HOMO-1 (2a'') \rightarrow N_2 LUMO ($1\pi_g$) donation	-61.6 (10.8%)
$\Delta E_{\text{orb}}(3)^{[b]}$	BBCO LUMO (11a') \leftarrow N_2 HOMO-1 ($1\pi_u$) donation	-108.0 (18.9%)
$\Delta E_{\text{orb}}(4)^{[b]}$	BBCO LUMO+4 (14a') \leftarrow N_2 HOMO ($3\sigma_g$) donation	-50.1 (8.8%)
$\Delta E_{\text{orb}}(5)^{[b]}$	BBCO LUMO+1 (3a'') \leftarrow N_2 HOMO-1 ($2\pi_u$) donation	-26.9 (4.7%)

[a] The values within the parentheses show the contribution to the total attractive interaction $\Delta E_{\text{elstat}} + \Delta E_{\text{orb}}$. [b] The values within parentheses show the contribution to the total orbital interaction ΔE_{orb} .

Table S8. EDA-NOCV results of I1 ($^1A'$) at the Hybrid/B3LYP/TZ2P level taking BBCO and N₂ in the different charged states as interacting fragments. Energy values are in kcal/mol.

Energy terms	BBCO (S) + N ₂ (S)	BBCO (T) + N ₂ (T)	BBCO ²⁺ (T) + N ₂ ²⁻ (T)	BBCO ⁴⁺ (S) + N ₂ ⁴⁻ (S)
ΔE_{int}	-114.4	-215.4	-871.0	-3195.3
ΔE_{Pauli}	740.6	1112.5	692.5	782.6
$\Delta E_{\text{elstat}}^{[a]}$	-283.2 (33.1%)	-387.4 (29.2%)	-924.4 (59.1%)	-2728.6 (68.6%)
$\Delta E_{\text{orb}}^{[a]}$	-571.8 (66.9%)	-940.4 (70.8%)	-639.1 (40.9%)	-1249.3 (31.4%)
$\Delta E_{\text{orb}}(1)^{[b]}$	-305.5 (53.4%)	-321.3 (34.2%)	-184.2 (28.8%)	-391.8 (31.4%)
$\Delta E_{\text{orb}}(2)^{[b]}$	-61.6 (10.8%)	-198.2 (21.1%)	-147.9 (23.1%)	-330.3 (26.4%)
$\Delta E_{\text{orb}}(3)^{[b]}$	-108.0 (18.9%)	-166.7 (17.7%)	-142.5 (22.3%)	-213.8 (17.1%)
$\Delta E_{\text{orb}}(4)^{[b]}$	-50.1 (8.8%)	-143.4 (15.2%)	-62.7 (9.8%)	-108.8 (8.7%)
$\Delta E_{\text{orb}}(5)^{[b]}$	-26.9 (4.7%)	-41.7 (4.4%)	-56.8 (8.9%)	-104.6 (8.4%)

[a] The values within the parentheses show the contribution to the total attractive interaction $\Delta E_{\text{elstat}} + \Delta E_{\text{orb}}$. [b] The values within parentheses show the contribution to the total orbital interaction ΔE_{orb} .

Table S9. The natural charge from Natural Population Analysis (NPA) throughout the generation process of BNBBCO from NNBBCO (see Fig. 3), calculated at the B3LYP/ def2-TZVPP level.


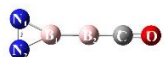
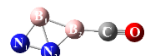


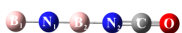
Natural Charge / e	N ₁	N ₂	B ₁	B ₂	C	O	CO	BB	NN
NNBBCO									
	0.105	-0.157	0.171	-0.263	0.518	-0.374	0.144	-0.092	-0.052
$(\eta^2\text{-N}_2)\text{BBCO}$									
	-0.205	-0.205	0.373	0.097	0.306	-0.366	-0.060	0.470	-0.410
I1									
	-0.464	-0.234	0.660	-0.178	0.571	-0.356	0.215	0.482	-0.698
I2									
	-0.540	-0.270	0.421	0.031	0.674	-0.317	0.357	0.452	-0.810
I3									
	-0.917	-0.219	0.441	0.408	0.595	-0.307	0.288	0.849	-1.136
BNBNCO									
	-1.316	-0.811	0.444	1.179	0.917	-0.414	0.503	1.623	-2.127

Table S10. The natural charge from Natural Population Analysis (NPA) throughout the generation process of BNNB + N₂ form NNBBNN (see Fig. S15), calculated at the B3LYP/ def2-TZVPP level.


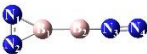

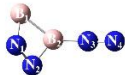


Natural Charge / e	N ₁	N ₂	B ₁	B ₂	N ₃	N ₄	N ₁ N ₂	BB	N ₃ N ₄
NNBBNN									
	0.088	-0.153	0.065	0.065	-0.153	0.088	-0.065	0.130	-0.065
$(\eta^2\text{-N}_2)\text{BBNN}$									
	-0.205	-0.205	0.342	0.409	-0.4	-0.06	-0.41	0.751	-0.46
I1									
	-0.514	-0.288	0.619	0.154	0.099	0.129	-0.802	0.773	0.228
I2									
	-0.534	-0.32	0.396	0.261	-0.009	0.207	-0.854	0.657	0.198
BNNB + N ₂									
	-1.264	-0.57	0.932	0.902	0	0	-1.834	1.834	0
									

Table S11. Calculated bond orders given by the Mayer method (MBO) and Wiberg method (WBO) at the B3LYP/def2-TZVPP level.

Complex	Mayer bond order	Wiberg bond order
NNBBCO		
N-N	2.10	2.89
N-B	1.29	1.55
B-B	1.94	1.91
B-C	1.47	1.54
C-O	2.22	2.86
(η^2-N₂)BBCO		
N-N	1.58	2.10
N-B	1.10	1.66
B-B	1.13	1.23
B-C	1.55	1.58
C-O	2.13	2.77
BNBNCO		
B ₁ -N ₁	1.25	1.97
N ₁ -B ₂	2.10	2.19
B ₂ -N ₂	1.41	1.65
N ₂ -C	1.99	2.21
C-O	2.16	2.88
BNCO		
B-N	1.18	1.95
N-C	1.98	2.20
C-O	2.18	2.90
NBCO		
N-B	2.63	2.95
B-C	1.24	1.46
C-O	2.35	2.97

Table S12. Orbital composition analysis on the BNBNCNCO complex by Natural Atomic Orbital (NAO) method.

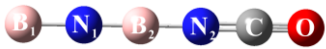
Complex	Orbital	Composition
BNBNCNCO 	HOMO	$B_1\ 2s\ (71\%) + 2p_z\ (24\%) + N_1\ 2s\ (3\%) + 2p_z\ (2\%)$
	HOMO-1	$B_1\ 2p_x\ (5\%) + N_1\ 2p_x\ (64\%) + B_2\ 2p_x\ (5\%) + N_2\ 2p_x\ (15\%) + C\ 2p_x\ (1\%) + O\ 2p_x\ (9\%)$
	HOMO-2	$B_1\ 2p_y\ (5\%) + N_1\ 2p_y\ (64\%) + B_2\ 2p_y\ (5\%) + N_2\ 2p_y\ (15\%) + C\ 2p_y\ (1\%) + O\ 2p_y\ (9\%)$
	HOMO-3	$B_1\ 2p_y\ (1\%) + N_1\ 2p_y\ (14\%) + B_2\ 2p_y\ (14\%) + N_2\ 2p_y\ (39\%) + O\ 2p_y\ (31\%)$
	HOMO-4	$B_1\ 2p_x\ (1\%) + N_1\ 2p_x\ (14\%) + B_2\ 2p_x\ (14\%) + N_2\ 2p_x\ (39\%) + O\ 2p_x\ (31\%)$
	HOMO-5	$B_2\ 2p_x\ (1\%) + N_2\ 2p_x\ (23\%) + C\ 2p_x\ (37\%) + O\ 2p_x\ (38\%)$
	HOMO-6	$B_2\ 2p_y\ (1\%) + N_2\ 2p_y\ (23\%) + C\ 2p_y\ (37\%) + O\ 2p_y\ (38\%)$

Table S13. EDA-NOCV results of BNB₂CO (¹Σ) at the Hybrid/B3LYP/TZ2P level taking [BNB⁺] (¹Σ) and [NCO⁻] (¹Σ) as interacting fragments. Energy values are in kcal/mol.

Energy terms	Orbital interaction	BNB ₂ CO (¹ Σ) [BNB ⁺] (¹ Σ) + [NCO ⁻] (¹ Σ)
ΔE_{int}		-304.4
ΔE_{Pauli}		337.1
$\Delta E_{\text{elstat}}^{[a]}$		-326.8 (50.9%)
$\Delta E_{\text{orb}}^{[a]}$		-314.8 (49.1%)
$\Delta E_{\text{orb}}(1)^{[b]}$	[BNB ⁺] 7σ ← [NCO ⁻] 7σ donation	-167.1 (53.1%)
$\Delta E_{\text{orb}}(2)^{[b]}$	[BNB ⁺] 2π ← [NCO ⁻] 2π donation	-45.2 (14.4%)
$\Delta E_{\text{orb}}(3)^{[b]}$	[BNB ⁺] 2π ← [NCO ⁻] 2π donation	-45.1 (14.3%)
$\Delta E_{\text{orb}}(4)^{[b]}$	[BNB ⁺] 7σ ← [NCO ⁻] 7σ donation	-50.2 (15.9%)

[a] The values within the parentheses show the contribution to the total attractive interaction $\Delta E_{\text{elstat}} + \Delta E_{\text{orb}}$. [b] The values within parentheses show the contribution to the total orbital interaction ΔE_{orb} .

Table S14. Experimental frequencies [cm⁻¹] of boron carbonyl compounds observed in a N₂ matrix.

Complex	CO	¹³ CO	C ¹⁸ O
OC ¹⁰ BCO	2017.9	1972.2	1992.8
OC ¹¹ BCO	2001.1	1956.3	1972.6
OC ¹⁰ B ¹⁰ BCO	2028.9	1978.4	2005.5
OC ¹¹ B ¹¹ BCO	2027.3	1976.8	1990.3

Table S15. Experimental frequencies [cm^{-1}] of boron nitrides observed in a N_2 matrix.

Complex	$^{14}\text{N}_2$	$^{15}\text{N}_2$
N^{10}BN	1644.7, 1637.7, 1570.7	1630.5, 1623.5, 1557.3
N^{11}BN	1590.1, 1518.7	1575.7, 1504.5
$^{10}\text{BN}^{10}\text{BN}$	2014.2, 2006.6, 2004.2	1982.6, 1974.8, 1972.5
$^{11}\text{BN}^{11}\text{BN}$	1960.4, 1958.1	1927.5, 1925.2
N^{10}BNN	2127.5, 2124.1, 1864.9, 1863.3	2057.4, 2054.2, 1845.6
N^{11}BNN	2127.5, 2124.1, 1807.3, 1805.8	2057.4, 2054.2, 1787.2, 1785.9
NN^{10}BNN	1988.6, 1819.5, 1231.4	1923.1, 1763.3, 1223.5
NN^{11}BNN	1988.6, 1819.5, 1186.8	1923.1, 1763.3, 1181.1
$\text{NN}^{10}\text{B}_2\text{NN}$	1933.0, 1180.5	1871.0, 1169.4
$\text{NN}^{11}\text{B}_2\text{NN}$	1931.4, 1151.5	1868.7, 1139.8
$\text{NN}^{10}\text{B}_3\text{N}_2$	1922.7, 1544.4	1860.2, 1540.9
$\text{NN}^{11}\text{B}_3\text{N}_2$	1921.7, 1480.0	1859.2, 1476.7
$\text{NN}^{10}\text{B}_4\text{NN}$	1937.0, 1189.6	1874.7, 1177.9
$\text{NN}^{11}\text{B}_4\text{NN}$	1935.4, 1142.6	1872.7, 1131.0

Table S16. Experimental frequencies [cm^{-1}] of the products of boron atom react with CO and N_2 in a N_2 matrix.

Complex	CO/ N_2	$^{13}\text{CO}/\text{N}_2$	$\text{C}^{18}\text{O}/\text{N}_2$	CO/ $^{15}\text{N}_2$
NN ^{10}BCO	2041.9, 1896.0	1957.1, 1890.8	2023.6, 1894.2	2030.4, 1854.5, 1830.1
NN ^{11}BCO	2036.4, 1889.7	1940.7, 1879.4	2002.9, 1882.6	/
$\text{N}_2^{10}\text{BCO}$	2079.0, 1597.1, 1181.3	2030.2, 1588.3, 1181.0	2050.1, 1592.3, 1177.0	2075.0, 1567.0, 1163.2
$\text{N}_2^{11}\text{BCO}$	2071.1, 1577.9, 1157.1	2022.1, 1576.8, 1154.7	2042.2, 1571.9, 1150.2	/
N $^{10}\text{BNCO}$	2315.5	2254.3	2297.1	2306.8
N $^{11}\text{BNCO}$	2314.8	2253.5	2297.2	/
$^{10}\text{B}(\text{NCO})_2$	2261.6	2210.5	2244.8	2252.6
$^{11}\text{B}(\text{NCO})_2$	2260.5	2198.7	2243.2	/

Table S17. Observed and calculated (at the B3LYP/def2-TZVPP and CCSD(T)/cc-pVDZ levels) infrared absorptions (cm^{-1}) for products **A-C** in the reactions of ^{11}B with CO in a N_2 matrix.

	Assignment	B3LYP/def2-TZVPP ^[a]	CCSD(T)/cc-pVDZ ^[b]	Obs.
(A) NNBBCO	NN, CO sym	2077.4	2082.2	/
	NN, CO asym	2058.3	1967.4	2047.5
	BB str	1672.6	1631.9	1626.7
	BB str	1080.8	1096.4	1113.6
(B) ($\eta^2\text{-N}_2$)BBCO	CO str	1995.8	2052.2	1997.2
	NN str	1591.8	1582.1	/
	BB str	1285.0	1295.9	1253.3
(C) BNBNC O	CO str	2356.0	2427.7	2334.1
	BN str	1989.0	2036.7	1986.5
	BN str	1569.1	1586.5	1547.2
	BN str	1197.8	1191.5	/

[a] Scaled frequencies using a scaling factor of 0.9661, which is obtained from the ratio of the experimental stretching frequency (2139 cm^{-1}) and the calculated value (2214 cm^{-1}) for CO. [b] Scaled frequencies using a scaling factor of 0.9977, which is obtained from the ratio of the experimental stretching frequency (2139 cm^{-1}) and the calculated value (2144 cm^{-1}) for CO.